**Low temperature properties of some $RIn_3$ compounds**

by

**Lucas Michael Hale**

A thesis submitted to the graduate faculty

in partial fulfillment of the requirements for the degree of

MASTER OF SCIENCE

Major: Materials Science and Engineering

Program of Study Committee:
Vitalij K. Pecharsky, Major Professor
Karl A. Gschneidner, Jr.
Alan M. Russell
Robert McQueeney

Iowa State University

Ames, Iowa

2007

# Table of Contents

# Abstract

The magnetic susceptibilities of $RIn_3$ compounds, where R represents the rare earth elements Y, Ce, Pr, Nd, and Dy have been measured. The susceptibilities found are consistent with literature values.

The low temperature heat capacity of $ErIn_3$ has been studied because of its potential for use as a low temperature regenerator material. Slight variations from stoichiometry have shown to affect the heat capacity of $ErIn_3$. Also, substituting some or all of the erbium with other rare earth elements causes the temperature at which the magnetic transformation occurs to shift. The $(Ho_xEr_{1-x})In_3$ system has been extensively studied. Some of these samples show anomalous behavior in both their lattice parameters and heat capacity values. In addition, several other $(R_xEr_{1-x})In_3$ samples have been measured for x = 0.05 and 0.1, and R = Y, Ce, Pr, and Dy. Finally, the heat capacity of $ErIn_3$ is found to be affected by physical deformation of the material.

# Chapter 1: General

## *1.1 Background and Literature Review*

### 1.1.1 $RIn_3$ compounds

#### *1.1.1.1 History of $RIn_3$'s*

The first $RIn_3$ compounds to be discovered were $PrIn_3$, $SmIn_3$, and $NdIn_3$. Iandelli [1] reported their existence in 1947, determined that they have the $AuCu_3$-type crystal structure, and established their lattice parameters. $CeIn_3$ was identified next in 1954 by Vogel and Klose [2]. Then, in 1960, Iandelli [3] announced that $LaIn_3$ was found, and Baenziger and Moriarty [4] reported on $GdIn_3$ and $DyIn_3$ in 1961. The rest of the $RIn_3$ family of intermetallics was investigated by Kuz'ma and Markiv [5] in 1963. The latter authors were the first to show the existence of the compounds containing Y, Tb, Ho, Er, Tm, Yb, and Lu and the non-existence of $EuIn_3$. All of the $RIn_3$ compounds were shown to have the $AuCu_3$ type structure, and the trend in the lattice parameters across the series was found to be consistent with other rare earth compounds, i.e. they exhibited the lanthanide contraction. Over the years, many other sources have confirmed the presence of these compounds and the magnitude of their lattice parameters [6-14]. Only $PmIn_3$ has not been experimentally confirmed due to promethium's radioactivity (the most stable isotope has a half-life around 17 years) although its existence has been predicted in some hypothetical phase diagrams [15-17].

### *1.1.1.2 Reported lattice parameters*

The lattice parameters of the rare earth compounds reported from various literature sources have been compiled in Table 1-1 and are plotted in Figure 1-1 as a function of the atomic number of the rare earth metal. It can be seen that there are some variations in the reported values for each compound. Considering that the elemental purity, sample preparation and XRD technique used to determine these values differ for all of the sources, it is expected that there should be some range in the lattice parameter values. However, can all of the variation be justified as resulting strictly from experimental errors? The maximum range in lattice parameters for one of these compounds is 0.0154 Å for $NdIn_3$. Although this difference is only 0.33%, it still is considerably higher than what is considered to be a typical experimental error for x-ray analysis, which is usually on the order of 0.005%.

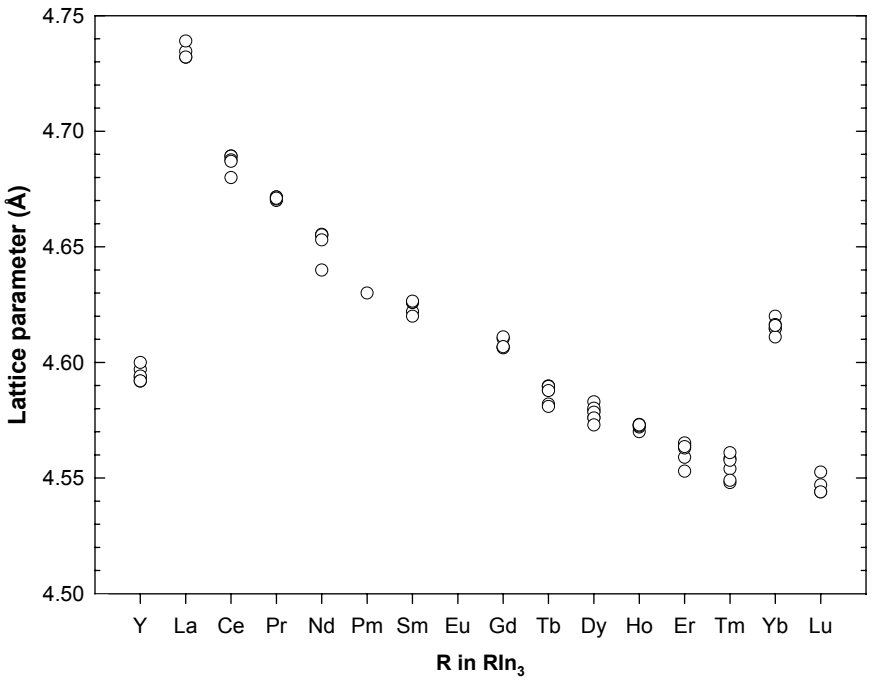


**Figure 1-1: The lattice parameters reported by various sources for the $RIn_3$ family of intermetallics [1-16].**

**Table 1-1: Lattice parameter values (Å) reported for the $RIn_3$ family of compounds.**

| | | | | | | | | |
|---|---|---|---|---|---|---|---|---|
| $YIn_3$ | 4.597 | [5] | $SmIn_3$ | 4.622 | [1] | $HoIn_3$ | 4.573 | [5] |
| | 4.5935 | [7] cast | | 4.6259 | [7] cast | | 4.57 | [6] |
| | 4.5941 | [7] anneal | | 4.626 | [7] anneal | | 4.5732 | [7] cast |
| | 4.5919 | [9] | | 4.6265 | [9] | | 4.572 | [7] anneal |
| | 4.592 | [11] | | 4.62 | [14] | | 4.5725 | [9] |
| | 4.6 | [14] | $GdIn_3$ | 4.6103 | [4] | | 4.573 | [12] |
| $LaIn_3$ | 4.732 | [3] | | 4.611 | [5] | $ErIn_3$ | 4.559 | [5] |
| | 4.7345 | [7] cast | | 4.6066 | [7] cast | | 4.563 | [6] |
| | 4.7321 | [9] | | 4.6063 | [7] anneal | | 4.5644 | [7] cast |
| | 4.739 | [11] | | 4.6068 | [9] | | 4.5652 | [7] anneal |
| $CeIn_3$ | 4.68 | [2] | $TbIn_3$ | 4.588 | [5] | | 4.5636 | [9] |
| | 4.6893 | [7] cast | | 4.5897 | [7] cast | | 4.553 | [14] |
| | 4.6892 | [7] anneal | | 4.5898 | [7] anneal | $TmIn_3$ | 4.554 | [5] |
| | 4.6876 | [9] | | 4.5896 | [8] | | 4.5584 | [7] cast |
| | 4.687 | [11] | | 4.5878 | [9] | | 4.5577 | [7] anneal |
| $PrIn_3$ | 4.67 | [1] | | 4.582 | [12] | | 4.561 | [8] |
| | 4.6716 | [7] cast | | 4.581 | [14] | | 4.548 | [9] |
| | 4.6715 | [7] anneal | $DyIn_3$ | 4.5762 | [4] | | 4.549 | [14] |
| | 4.6707 | [9] | | 4.583 | [5] | $YbIn_3$ | 4.62 | [5] |
| | 4.671 | [13] | | 4.5791 | [7] cast | | 4.6146 | [7] cast |
| $NdIn_3$ | 4.655 | [1] | | 4.5802 | [7] anneal | | 4.6147 | [7] anneal |
| | 4.6554 | [7] cast | | 4.5785 | [9] | | 4.6164 | [8] |
| | 4.6551 | [7] anneal | | 4.576 | [10] | | 4.611 | [9] |
| | 4.653 | [9] | | 4.573 | [14] | | 4.616 | [11] |
| | 4.64 | [14] | | | | $LuIn_3$ | 4.544 | [5] |
| $PmIn_3$ | 4.63 | [16] theor. | | | | | 4.5526 | [7] cast |
| | | | | | | | 4.547 | [11] |
| | | | | | | | 4.544 | [14] |

### *1.1.1.3 Reported magnetic properties*

One of the best ways of determining the magnetic properties of a material is by measuring its magnetic susceptibility. Magnetic susceptibility, $\chi$, is defined as the magnetization of the material, $M$, divided by the applied magnetic field, $H$:

$$\chi = \frac{M}{H}$$

The behavior of the susceptibility as a function of temperature is different for the different magnetic behaviors.

The susceptibility of conventional paramagnetic materials will behave in one of two ways: either it will follow the Curie law or it will be independent of temperature, which is known as Pauli paramagnetism. The Curie law states that the susceptibility is related to the temperature by:

$$\chi = \frac{C}{T}$$

where $T$ is the absolute temperature and $C$ is the Curie constant for that material. When analyzing data, it is often more useful to look at the reciprocal susceptibility:

$$\frac{1}{\chi} = T\frac{1}{C}$$

For materials that follow the Curie law, plotting the reciprocal susceptibility vs. the temperature should result in a straight line with the slope being the inverse of the Curie constant.

The Curie constant is a value that is unique for each material. The Curie constant is given by:

$$C = \frac{\mu_0 n m^2}{3k_B}$$

where $\mu_0$ is the permeability of free space, $n$ is the number of atoms per unit volume, $k_B$ is Boltzmann's constant, and $m$ is the magnetic moment per atom. The value of $n$ can easily be

determined if the unit cell structure and lattice parameters of a material are known. This allows for the magnetic moment to be determined experimentally using the Curie constant. The magnetic moment per atom calculated from the Curie constant is dependent on the effective magnetic moment, $p_{eff}$, of the different atoms composing the material. The effective magnetic moment is the magnetic moment that is created by one atom or ion of a specific type. If the interaction between atoms in a solid does not change the effective magnetic moment of the atoms, then the magnetic moment squared per unit volume of a material is the sum of the $(p_{eff})^2$ of all the atoms in that volume.

For a given ion, the effective magnetic moment is dependent on the number of unpaired electrons and can be theoretically calculated using quantum theory. For the lanthanides, the 4*f* shell of electrons is the most important for the magnetic properties. The unpaired 4*f* electrons result in the atom having non-zero orbital and spin angular momentum quantum numbers. The sum of these two angular quantum numbers is known as the total atomic angular momentum quantum number, *J*. The $p_{eff}$ of rare earth elements is then calculated using:

$$p_{eff} = g\sqrt{J(J+1)}$$

The quantity *g* is known as the spectroscopic splitting factor and is given by:

$$g = 1 + \frac{J(J+1) + S(S+1) - L(L+1)}{2J(J+1)}$$

where *L* is the orbital angular momentum quantum number and *S* is spin angular momentum quantum number [31, 36].

The Curie law can also help with the identification of the ground state of ferromagnetic and antiferromagnetic materials. For these materials, the ordered magnetic structure is not present for all temperatures and above a certain temperature characteristic for that material, it will become paramagnetic. Above this transition temperature, the relationship between the reciprocal susceptibility and temperature is still linear. This allows for a modified version of the Curie law, called the Curie-Weiss law to be used:

$$\chi = \frac{C}{(T - \theta_C)}$$

where $\theta_C$ is a constant known as the Weiss temperature. For ferromagnetic materials, the Weiss temperature is positive, and it approximately coincides with the temperature (Curie temperature, $T_C$) at which the paramagnetic-ferromagnetic transformation occurs.

Things are slightly more complicated for antiferromagnetic materials. The reciprocal susceptibility is still linear above the paramagnetic-antiferromagnetic transition. In these materials, the transition temperature is called the Néel temperature, $T_N$, and does not occur at the Weiss temperature as defined in the Curie-Weiss law. In fact, if the paramagnetic regime is extrapolated, the corresponding Weiss temperature constant for these materials is found to be negative. Because of this, for simple antiferromagnetic materials, there are two distinguishing temperature values: the Néel temperature and the Weiss temperature. Although these two values are different, for many materials $T_N \approx |\theta_C|$.

The first comprehensive study of the magnetic susceptibilities of the $RIn_3$ compounds was published by Buschow, et al. [9] in 1969. Nearly all of the compounds (R = Ce, Nd, Sm, Gd,

Tb, Dy, Ho, and Er) were found to order antiferromagnetically at low temperatures (Figure 1.2), and all except for R = La, Sm, Y, and Yb follow the Curie-Weiss behavior at high temperatures. $YIn_3$ and $LaIn_3$ were found to be Pauli paramagnetic. $PrIn_3$ follows the Curie-Weiss behavior down to about 30 K at which point there is a deviation due to crystalline electric field effects. No magnetic transition was found in$TmIn_3$ down to 2.5 K. Graphs of the reciprocal susceptibility vs. temperature are show in Figure 1-2.

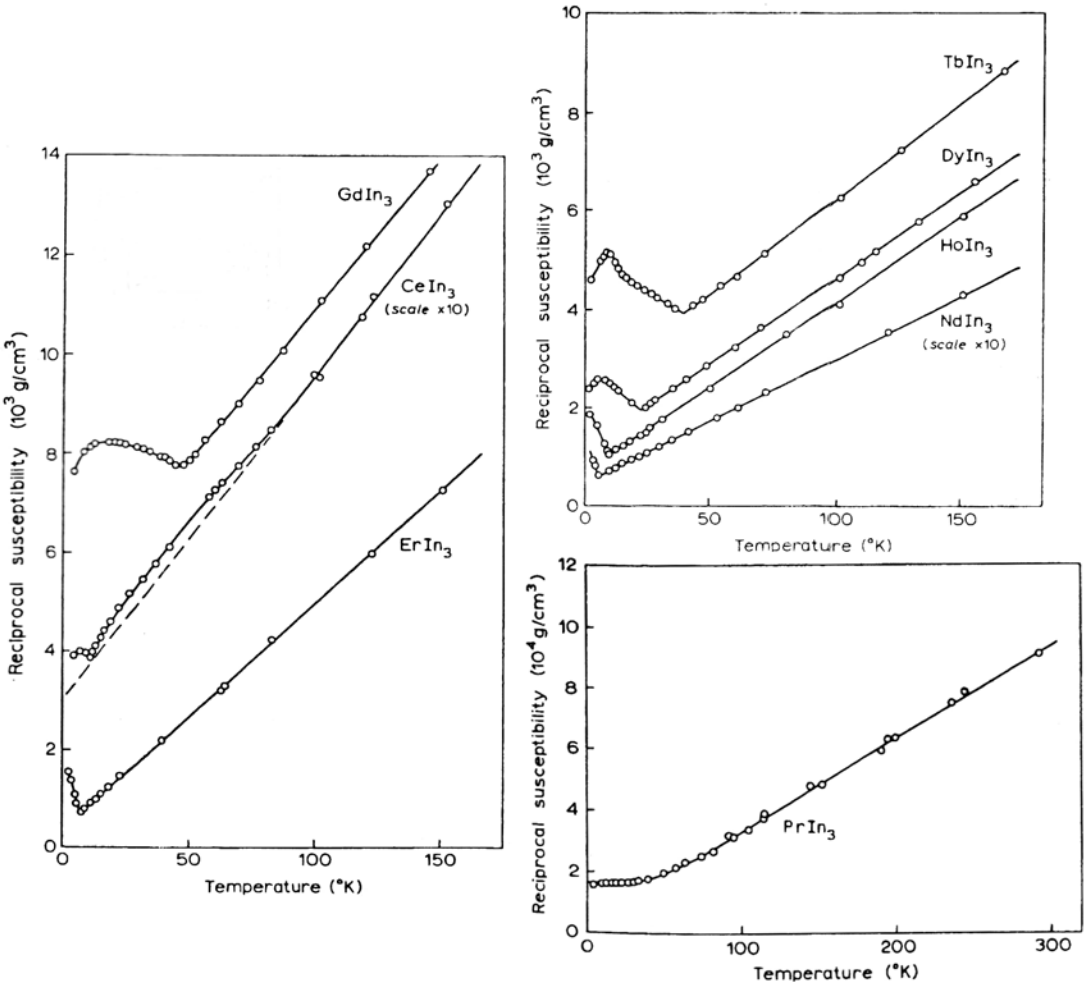


**Figure 1-2: Reciprocal susceptibility vs. temperature graphs for many of the $RIn_3$ compounds as determined by Bushow et al. [9].**

The Néel temperatures and Weiss temperature constants reported for the $RIn_3$ compounds from various sources are shown in Table 1-2. If the source used a technique other than normal magnetic type measurements to determine the Néel temperature, then the method is listed in the table.

**Table 1-2: A summary of the Weiss temperature constants, Néel temperatures and effective magnetic moments for the $RIn_3$ compounds previously reported. If no method is listed, the sources used the normal magnetic type measurements to determine the values. "Single Crystal" refers to magnetic susceptibility measurements of single crystals.**

| Compound | $\theta c$ | $T_N$ | $p_{eff}$ | Notes | Source |
|---|---|---|---|---|---|
| $YIn_3$ | | Pauli P | | | [9] |
| $LaIn_3$ | | Pauli P | | | [9] |
| $CeIn_3$ | -46 | 11 | 2.54 | | [9] |
| $PrIn_3$ | -10 | --- | 3.58 | | [9] |
| | -9 | --- | 3.72 | | [34] |
| $NdIn_3$ | -17 | 7 | 3.62 | | [9] |
| | -12 | 6.8 | 3.78 | | [34] |
| | | 7 | | Single Crystal | [33] |
| $SmIn_3$ | | 16 | | | [9] |
| $GdIn_3$ | -85 | 45 | 8.02 | | [9] |
| | | 42-44 | | Single Crystal | [33] |
| $TbIn_3$ | -62 | 36 | 10.05 | | [9] |
| | | 37 | | Neutron Diffraction | [12] |
| $DyIn_3$ | -35 | 23 | 10.78 | | [9] |
| | | 24 | | Neutron Diffraction | [10] |
| | | 18.5-20 | | Single Crystal | [33] |
| $HoIn_3$ | -18 | 11 | 10.65 | | [9] |
| | | 11.5 | | Neutron Diffraction | [12] |
| | | 7.92 | | Heat Capacity | [28] |
| $ErIn_3$ | -10 | 6 | 9.75 | | [9] |
| | | 4.86 | | Heat Capacity | [28] |
| $TmIn_3$ | -6 | --- | 7.6 | | [9] |
| $YbIn_3$ | | --- | | | [9] |

There are a few things to note in Table 1-2. First of all, "Single Crystal" refers to measuring the magnetic susceptibility of single crystals of the material. The range of Néel temperatures reported for the single crystals of $GdIn_3$ and $DyIn_3$ are due to the susceptibility being

dependent on the crystal's orientation. The other thing to be noticed is that the heat capacity measurements on $HoIn_3$ and $ErIn_3$ show the transition to occur at lower temperatures than the susceptibility measurements with $HoIn_3$ having a difference of over 3 K and $ErIn_3$ differing by approximately 1 K.

### 1.1.2 $(Ho_xEr_{1-x})In_3$

The amount of focus placed on the $(Ho_xEr_{1-x})In_3$ family of materials is due to early tests showing that these compounds have the potential for being used as regenerator materials in cryogenic regenerative heat exchangers, also known as regenerative cryocoolers. Regenerative cryocoolers are devices that use a cyclic process to cool target chambers down to low temperatures (generally <50K). Recent advancements have allowed relatively small commercial regenerative cryocoolers to reach temperatures of only a few degrees Kelvin.

#### *1.1.2.1 Regenerative Heat Exchangers*

There are various designs of regenerative heat exchangers, but they all have two things in common: they realize heat exchange, and they contain a regenerator. The regenerator is a chamber that contains a material with a high heat capacity that allows refrigeration at lower than normal temperatures by storing heat energy before or during the refrigeration cycle. To reach low temperatures, having a matrix material with a high heat capacity is a must as the heat capacity is a measure of how much heat the material can "store" per degree. The regenerator and regenerator materials are discussed more in depth in section 1.1.2.1.1.

The method of refrigeration carried out in the heat exchanger defines the type of cryocooler. Although knowledge of the different types of regenerative cryocoolers is not necessary for understanding the research presented here, it is useful to be aware of the different processes when viewing related works. Because of this, a brief overview of the most common types of regenerative cryocoolers is presented here. A more in-depth review can be found in Ackermann [18].

The majority of commercial regenerative cryocoolers use gas expansion and compression cycles to accomplish the refrigeration, but the specifics are dependent on the type. The three most common types of gas-based commercial regenerative cryocoolers are Stirling, Gifford-McMahon and pulse tube.

Stirling cryocoolers are devices that manipulate the coolant fluid mechanically through the use of a piston and a displacer that are contained within the same cylindrical chamber. The displacer separates what is known as the cold end chamber from the hot end, and the regenerator surrounds the piston so that the only way for the fluid to go from the hot chamber to the cold chamber is through the regenerator. Since everything is contained within one cylinder, these devices are ideal for applications that require small size and high efficiency [18].

In a refrigeration cycle for the Stirling cryocooler, the fluid starts in the hot end chamber. It is compressed by the piston, and the heat due to the compression is removed. Next, the displacer pushes the fluid through the regenerator to the cold-end chamber. Once at the cold

end, the piston moves out to expand the gas which cools it and allows it to absorb heat from the chamber being refrigerated. Finally, the displacer moves back to where it initially started returning the fluid to the hot end chamber via the regenerator.

The principles behind Gifford-McMahon cryocoolers are essentially the same as with Stirling except that the Gifford-McMahon cryocoolers use an inlet valve and an outlet valve in conjunction with the compressor. The refrigeration cycle is the same as for the Stirling cryocoolers except that the gas compression is done by opening the inlet valve to fill the system with high pressure gas and the expansion is done by opening the outlet valve to release the excess pressure. Another major difference is that the regenerator is usually contained in a separate chamber in the Gifford-McMahon cryocoolers as opposed to being contained within the same cylinder as usually is the case for the Stirling cryocoolers. Having the regenerator in the second chamber increases the size of the device slightly, but prevents vibrational problems that can arise in Stirling cryocoolers. [18,19]

Pulse tube cryocoolers operate differently than the other two types of cryocoolers in that no displacer is used to separate and move the fluid between the cold end and the hot end. Instead, the hot and cold heat exchangers are located on two sides of a tube that is closed on one side known as a pulse tube. Since there is nothing physically separating the two ends of the pulse tube, the fluid must flow through the regenerator before reaching the pulse tube. This differs from the Stirling and the McMahon cryocoolers where the fluid flows through the regenerator as it moves from the cold end to the hot end and vice versa. [18,19]

A cycle for the pulse tube cryocooler starts with the creation of a high pressure pulse of the cooling gas that is sent through the regenerator to the pulse tube. Since the pulse tube is closed on one end, the pressure in the tube increases and compresses the gas. Heat is then expelled through the hot heat exchanger located at the closed end of the tube. Next, the pressure in the system is reduced causing the gas in the pulse tube to expand. This results in cooled gas flowing towards the open end of the pulse tube where the cold heat exchanger is located allowing heat to be taken from the target chamber by the gas. [18,19]

#### 1.1.2.1.1 Properties of regenerator matrixes

The regenerator is a chamber within the cryocooler through which the fluid flows at some point in the refrigeration process. The purpose of the regenerator is to allow the refrigeration to be done at lower than normal temperatures by storing heat. This is done through the use of a high heat capacity material within the regenerator known as the regenerator material or the matrix material.

During the cycle of the cryocooler, the coolant fluid flows through the regenerator first in one direction and then the other. Over time, this creates a temperature gradient within the regenerator from one side to the other with the temperatures of the two ends being quite different from one another. Due to the temperature gradient, when the fluid flows from the hot end of the regenerator to the cold end, it is always in contact with matrix material that is at a lower temperature than the fluid resulting in the temperature of the fluid dropping drastically. Once the fluid is cooled by the regenerator, the refrigeration process can be

executed at temperatures near the temperature of the cooled fluid thus allowing for cooling at low temperatures.

In order for the fluid to be cooled while traveling through the regenerator, heat must be removed. However, that heat must go somewhere. As the regenerator cools the fluid, heat is being transferred from the fluid to the regenerator matrix thus increasing the temperature of the matrix. To return the matrix to its initial temperature gradient so that it can retain its effectiveness, the fluid must be sent back through the regenerator from the cold end to the hot end to heat the fluid and cool the matrix. The heat in the fluid is passed through a heat exchanger to remove and exhaust the heat to the ambient atmosphere. This necessary recovery step is the reason why the regenerator is said to store heat and why the total cooling process must be cyclical.

When it comes to the design of the regenerator, a number of things must be considered to maximize the regenerator's effectiveness. To be efficient, heat must be easily transferred between the matrix and the fluid with as little heat loss as possible occurring within the regenerator. The surface area of the regenerator matrix must be maximized to allow as much contact with the fluid as possible, but the shape of the material must also minimize pressure changes within the fluid. In addition, heat transfers through the outer casing of the regenerator and along the regenerator's transverse direction (the direction of the temperature gradient) also cause inefficiencies. The temperature gradient also causes problems due to changing the pressure and viscosity of the fluid and the heat capacity of the matrix. For an

in-depth view of these sources of efficiency losses and their importance, see Ackermann [18].

The most important property for identifying a possible regenerator matrix material is a high volumetric heat capacity. As the regenerative process cycles, the matrix material stores and releases heat, thus changing temperature. The difference between the maximum and minimum temperature of a given point in the matrix during one cycle is known as the temperature swing. The smaller the temperature swing, the more efficient the regenerator is. By finding a material that has a high heat capacity, it can be insured that the temperature swing will be small.

While the high heat capacity allows potential regenerator matrix materials to be recognized, cost is also a major factor in determining the likelihood of those materials being used for commercial regenerative heat exchangers. The cost of creating a matrix material is dependent on the cost of the raw materials, ease of synthesis, ease of processing and any safety issues related to the handling of the material.

#### 1.1.2.1.2 Other regenerator materials

For reaching temperatures above 30 K the choice of regenerator matrix materials is simple. Copper, bronze and stainless steel are the most commonly used materials as they all have a high heat capacity around room temperature, are inexpensive and are easy to shape and process. It is easy to form these materials into wire screens allowing the porosity to be tightly controlled. Due to their effectiveness and low cost, there is no effort necessary for

replacing these materials. However, since they are simple metals, their total heat capacity is almost completely dependent on their lattice heat capacity.

The lattice heat capacity of materials is based upon the energy of lattice vibrations. At high temperatures, the constant volume heat capacities of most solids approaches 3R while at low temperatures the heat capacity becomes strongly temperature dependent and drops to 0 with a $T^3$ dependence. The use of quantum mechanics was necessary to obtain an accurate model of this behavior over the whole temperature range. The equation for this model is known as the Debye equation and is given by:

$$C_V = 9R\left(\frac{T}{\theta_D}\right)^3 \int_0^{\theta_D/T} \frac{x^4 e^{-x}}{\left(1-e^{-x}\right)^2} dx \qquad x = h\nu / k_B T$$

where $\theta_D$ is a parameter known as the Debye temperature that is used to fit the model to data. Roughly, the Debye temperature represents the temperature below which the material's heat capacity becomes highly temperature dependent. Therefore, at low temperatures, a material with a low Debye temperature will have a higher heat capacity than a material with a high Debye temperature. The experimental heat capacities of a few elements and their corresponding Debye fits are shown in Figure 1-3 [20].

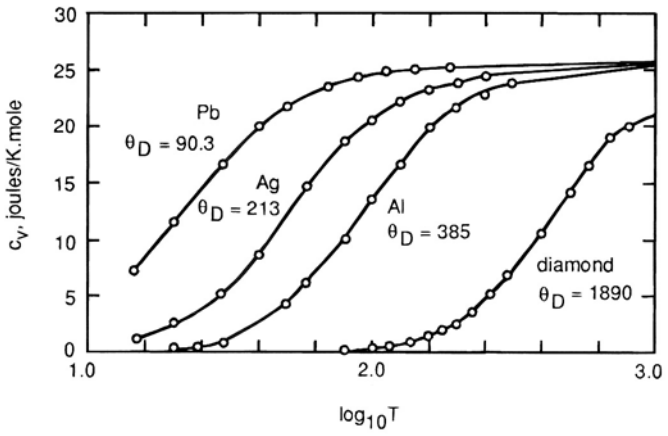


**Figure 1-3: The constant volume heat capacity as a function of temperature for some materials. The circles represent experimental data and the lines are the Debye fit using the Debye temperatures shown. This graph is taken from [20].**

To achieve low regenerator temperatures with the above materials, the first step was to use materials with a low Debye temperature. Whereas copper has a Debye temperature above 300 K, lead has one about 90 K. This allows lead and lead compounds to be more effective below 30 K than the other metals. However, the use of lead does have limitations. First, the heat capacity still drops quickly with decreasing temperature below lead's Debye temperature limiting lead's use to above 10 K. Also, lead is too soft to retain any complex forms and, therefore, is limited to being formed as spheres. Finally, the safety concerns related to the use of lead have started a search for replacement materials.

Reaching temperatures below 10 K through the use of a regenerator requires that concepts besides lattice heat capacity are necessary to achieve high heat capacity materials within this range. One way of doing this is to find materials that undergo phase transitions within the wanted temperature range since the heat capacity of materials experience anomalous peaks

during phase transitions. The regenerator must be a solid requiring the phase transition to be solid to solid. However, kinetics at this temperature range would prevent any structural phase changes from being quick and useful. This leaves magnetic transitions as a viable possibility. Rare earth elements and many rare earth compounds undergo magnetic transitions making them ideal candidates for potential regenerator materials.

The first use of a rare earth compound as a low temperature regenerator material was in 1971 by Daniels and du Pre [21]. A regenerative cryocooler using just lead was tested to find its lowest level temperature. Two tests were then performed by replacing some of the lead at the low temperature end by first charcoal and then EuS. The idea for using the charcoal is that it is able to absorb helium gas to the point that the density of the helium within the charcoal is near the density of liquid helium. If the heat capacity of the absorbed helium is close to that of the gas or liquid, then it should have a higher heat capacity than lead below 10 K. EuS was chosen because it has a heat capacity peak at 16 K allowing it to have a higher heat capacity than lead below 16 K. Both substitutions allowed the regenerator to reach slightly lower temperatures than lead alone, and the EuS regenerator showed the most improvement over the original.

In 1975, Buschow, et al. [22] was one of the first to attempt to engineer a rare earth intermetallic so that it has a high heat capacity between 4 and 10 K. The work started with the creation of 11 different GdA compounds where A is a transition metal. Most of these compounds were ferromagnetic, but three were antiferromagnetic. Using these results, the authors attempted to create an alloy that has a Curie temperature near 0 K by combining one

of the ferromagnetic alloys (GdA) with one of the antiferromagnetic alloys (GdA') to create a $GdA_xA'_{1-x}$ compound. These samples failed to produce a low temperature transition and instead kept both of the original ferromagnetic and antiferromagnetic transition peaks.

Next, the effect of varying the rare earth element of these compounds was investigated. Seeing that GdRh had the lowest transition temperature for the GdA compounds, RRh samples were created where R = Tb, Dy, Ho, and Er. The Tb and Dy showed lower ferromagnetic transition temperatures than GdRh while HoRh and ErRh both showed low temperature antiferromagnetic transformations. Tests were then done to see how the peaks were affected across the pseudo binary system between GdRh and ErRh. As the composition changed, the peaks broadened and eventually became one wide double peak. From this, it was shown that the heat capacity peaks of rare earth compounds could be manipulated by changing the rare earth content of intermetallics. However, the high cost of rhodium prevents these compounds from being used in commercial applications.

The next big breakthrough for the use of rare earth compounds as regenerator matrixes would not happen until 1990. Sahashi, et al. [23] and Kuriyama, et al. [24] saw that $Er_3Ni$ undergoes a transition near 7 K and the peak is rather broad. This peak makes the heat capacity of $Er_3Ni$ much higher than lead below 15 K. In addition to this, the heat capacity above 15 K is only slightly lower than lead. They showed that identical spheres of the material could be produced by the use of the Rotating Disk Atomization Process. Finally, the spheres that were produced were used to replace some of the lead at the cold end of a second stage regenerator. The regenerator using the $Er_3Ni$ compound was shown to be more

efficient and reached a lower temperature than an identical regenerator using only lead. This study resulted in the first commercial regenerator using rare earth compounds as a low temperature regenerator material.

Since $Er_3Ni$, many other compounds have been found as possible substitutes. Biwa, et al. [25] proposed the use of a combination of different Er-Ag compounds in series within the regenerator. If they are used together and in the proper location, higher heat capacities than lead are reached above 25 K and below 15 K. The Er-Ag alloys also were shown to have higher heat capacities than $Er_3Ni$ everywhere except at $Er_3Ni$'s peak. The downside to these compounds is that there is no single alloy that has a higher heat capacity for the entire range.

Satoh, et al.[26] used a combination of lead, $HoCu_2$ and $NdInCu_2$ within a G-M cycle cryocooler to reach temperatures below 2K in 2001. $HoCu_2$ experiences a broad double peak between 5 and 10 K, while $NdInCu_2$ peaks at 2K. In order to reach temperatures below 2 K, the normal $^4He$ fluid was replaced by $^3He$.

Also in 2001, Gschneidner, et al.[27] proposed the use of impure erbium and Er-Pr alloys as possible substitutes for lead. The heat capacity for erbium, both pure and impure is greater than lead between 20 and 80 K and approximately the same outside that range. The high heat capacities between 20 and 80 K are due to magnetic transitions in Er at 19, 25 and 52 K. The addition of Pr in these studies was done hoping that the sharp peak at 19 K in pure Er could be shifted and broadened to improve the heat capacity below 20 K. Although this alloying was effective for below 20 K, it also shortened the temperature range above 20 K for which

erbium has a higher heat capacity than lead. For this reason, the paper suggests using a combination of different alloys to maximize the heat capacity for the entire range below 80 K although almost all of the alloys alone have a heat capacity higher or nearly equal to that of lead for that range. Also, these compounds are alloys and not intermetallics and are therefore ductile and stronger than lead allowing them to possibly be used in non-spherical forms.

#### *1.1.2.2 $Ho_xEr_{1-x}In_3$ background*

The holmium-indium and erbium-indium phase diagrams are very similar, as can be seen in Figures 1-4 and 1-5. There is almost no solubility of either rare earth element in pure solid indium. Also, the $RIn_3$ compound is the first intermetallic compound to form on the indium-rich side of the systems. Any sample that contains more than 75 at% indium will contain pure indium along with the $RIn_3$ compound.

The low temperature heat capacities of $ErIn_3$ and $HoIn_3$ were first studied by Czopnik, et al. in 1986 [28]. This research showed that the Néel temperatures for the two compounds from the heat capacity measurements were slightly lower than those determined by Bushow, et al. [22] from magnetic susceptibility data. $ErIn_3$ reaches its transition at 4.86 K and $HoIn_3$ orders at 7.92 K. The heat capacity peak for $ErIn_3$ was shown to be very sharp and narrow with a maximum heat capacity of 1.76 J/cm$^3$K. The peak in $HoIn_3$ is broader due to what appears to be a second magnetic transition peak occurring at 7.7 K, however, the maximum heat capacity is only 0.88 J/cm$^3$K.

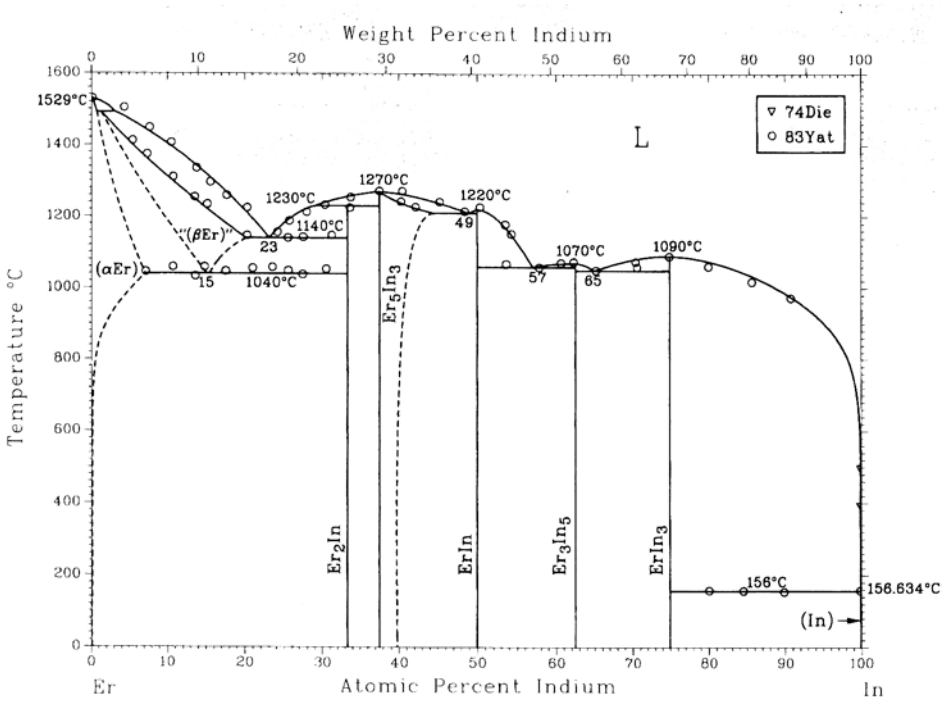


**Figure 1-4: The erbium-indium phase diagram [17].**

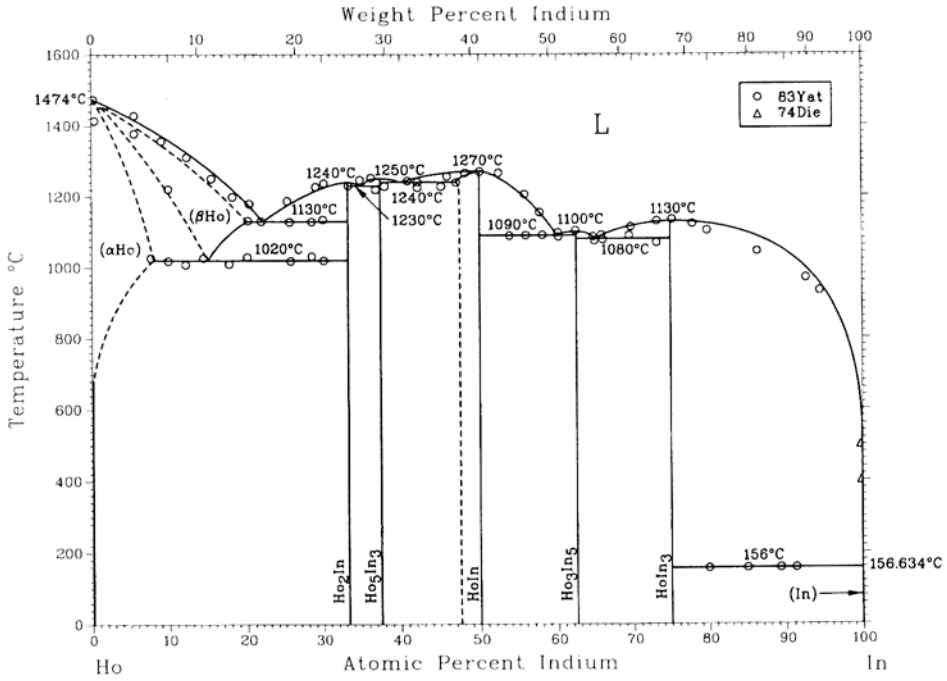


**Figure 1-5: The holmium-indium phase diagram [17].**

The use of these elements as regenerator matrix materials would not be explored until nearly twenty years later in early 2006 by Gschneidner, et al. [29]. The heat capacities and lattice parameters were measured for $ErIn_3$ and $HoIn_3$ along with five intermediate alloys of $(Ho_xEr_{1-x})In_3$.

The intermediate alloys were prepared to determine the effects that the varying composition has on the properties. While the magnitudes of the heat capacity peaks of $HoIn_3$ and $ErIn_3$ are quite large, they are also very narrow severely limiting the range of their effectiveness. By manipulating the composition, the hope was to obtain one or more intermediate compositions with a heat capacity peak in the temperature range between the two end compounds as had been done for other families of regenerator matrices.

The results of this work were not expected, to say the least. While the measurements of $HoIn_3$ were all consistent with previous results, the measurements of $ErIn_3$ were not. First, the heat capacity measurement of the pure $ErIn_3$ was quite different than what Czopnik et al. reported. The Néel temperature was found to occur at 4.45 K, and the peak only had a maximum heat capacity of 0.88 $J/cm^3K$, nearly half of what was earlier reported. Also, the lattice parameter for $ErIn_3$ varied enough from the literature value cited to be worth mentioning. These discrepancies in the properties of $ErIn_3$ led to the suggestion that it is possible there is a slight solid solubility around the exact stoichiometry due to substitution between erbium and indium atoms. This substitution of atoms in the crystal structure is a distinct possibility because of the similarity in the atomic radii of the two atoms and the fact

that both are trivalent. It was also suggested that impurities could also be the reason for the differences in the properties.

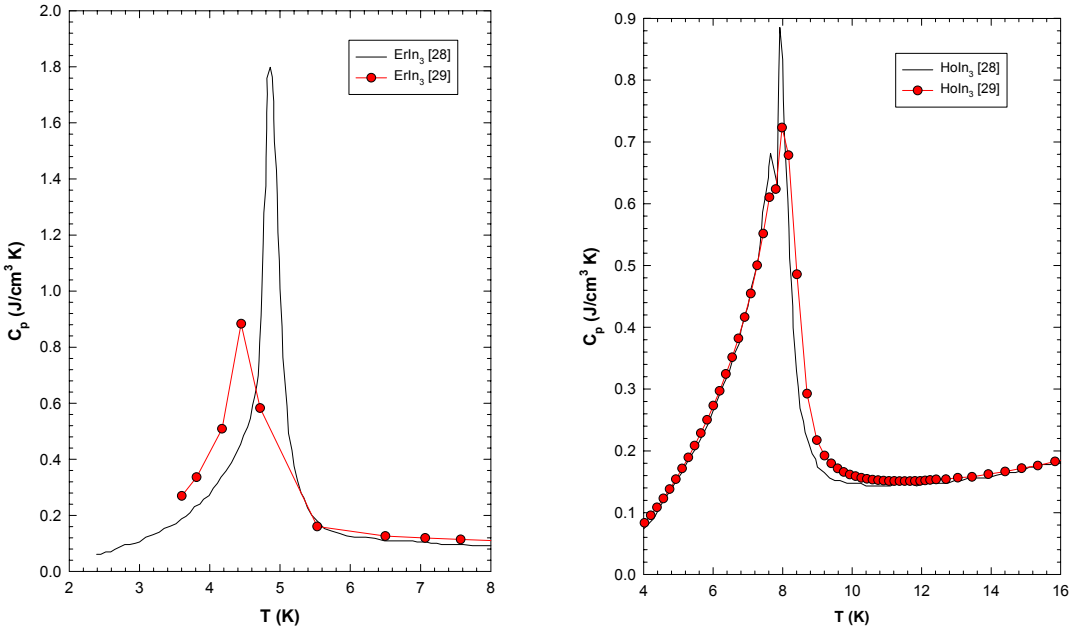


**Figure 1-6: The reported temperature dependent heat capacities of $ErIn_3$ and $HoIn_3$. Note that the heat capacity is nearly the same for $HoIn_3$ but quite different for $ErIn_3$.**

The results for the intermediate compounds also differed greatly from what was expected. Instead of following a simple linear trend across the compound series, there is a substantial dip in both the lattice parameter and Néel temperature values for the compositions x = 0.3, 0.35 and 0.5 of $(Ho_xEr_{1-x})In_3$. This can be seen in Figure 1-7.

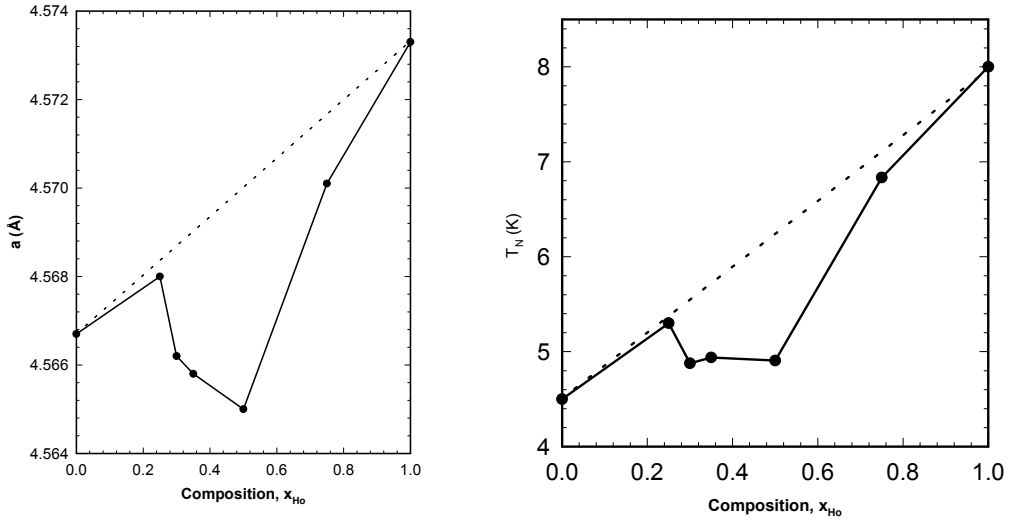


**Figure 1-7: The compositional dependence of the lattice parameter and Néel temperature for the $(Ho_xEr_{1-x})In_3$ compounds [29].**

## *1.2 Experimental Procedures*

### 1.2.1 Sample Preparation

The indium used was greater than 99.9% pure. Two types of erbium were used. The first type was obtained from the Materials Preparation Center, MPC, of Ames Laboratory and was 99.8+ at% pure. The other was commercial grade, "99.9% pure" erbium that is approximately 94 at% pure with most of the impurity due to oxygen and carbon contents. All the other rare earth elements were obtained from the Materials Preparation Center of Ames Laboratory and were at least 99.8 at% pure.

All of the arc-melted samples were prepared identically. First, the individual components were weighed to within ±0.0002 grams of the intended stoichiometry. The components were melted on a water cooled copper hearth under an argon environment. After melting, the

samples were flipped and remelted five times to ensure a homogeneous composition. The differences between the before and after melting weights were less than 1% and deemed negligible. None of the arc-melted ingots was heat treated as bulk samples since they were found to be single phase (in some cases with slight traces of indium.)

In addition to arc-melting, some of the $ErIn_3$ samples were prepared using an induction furnace. The details of this are explained later in the results.

### 1.2.2 X-ray measurements

X-ray powder diffraction was performed on all of the samples prepared to ensure that the samples were single phase and to determine the lattice parameters. In addition, the samples that were used in the previous study by Gschneidner, et al. [29] were re-examined and the lattice parameters recalculated. The samples from that work had been prepared in exactly the same manner as those first presented here using the same equipment and base materials.

The samples were ground into a powder using a pestle and mortar and were heat treated at 600°C for 1 hour to relieve stress. A Scintag powder diffractometer using Cu Kα radiation was used to evaluate the samples with data collected from 20° to 120° 2θ with a step size of 0.02° and a scan time of 5 seconds for each step. The lattice parameters were then refined from the data using LHPM Rietica software [30]. More details on the heat treating and choice of measurement angles can be found in the results section of this document.

### 1.2.3 Susceptibility measurements

The magnetic susceptibilities of the alloys were determined using a Lakeshore Magnetometer/Susceptimeter or a SQUID Magnetometer. Both instruments were used to determine the susceptibility of the $RIn_3$ compounds presented here. While the Lakeshore unit was capable of measuring the samples that contained erbium, holmium and dysprosium, it was not sensitive enough to measure the other $RIn_3$ samples; for these the SQUID was used. [31]

There were two methods used by these instruments to determine the susceptibility of the compounds. The first was to use an alternating current to produce a varying field and to measure the susceptibility directly. The second was to use a constant direct current electric field to produce a constant magnetic field and measure the sample's magnetization at different temperatures. The susceptibility is then found to be the magnetization divided by the magnetic field at any given temperature.

### 1.2.4 Heat capacity measurements

The heat capacity was measured using a fully automatic semiadiabatic heat-pulse calorimeter as described by Pecharsky, et al. [32]. Most of the samples used were rectangular sections cut out of the bulk ingots. The two sides that were not cut were polished flat and parallel using dry sand paper of different grit sizes with the finest being 600 grit. The final weight of the samples was approximately 1-2 g. Other samples were prepared by pressing $ErIn_3$ powder together to form a cylinder of approximately 1 g.

From thermodynamics, the heat capacity at constant pressure is defined by

$$C_P = \left(\frac{\partial Q}{\partial T}\right)_P$$

For small changes in the temperature, the heat capacity can be estimated as

$$C_P \cong \left(\frac{\Delta Q}{\Delta T}\right)_P$$

Where ΔQ is the amount of heat added to the sample from a heat pulse and ΔT is the corresponding change in temperature of the sample. Therefore, the heat capacity can be determined by measuring the temperature change resulting from a known pulse of heat. [32]

When determining the change in temperature, it must be realized that no matter how insulated the device is, there will still be a small amount of heat that will be transferred to the sample from the surroundings. This small amount of transferred heat means that the temperature of the sample between the known heat pulses will not be constant. If the heat flow into the calorimeter is sufficiently small, it can be assumed that this flow is steady over time and that the resulting temperature change is small enough that the heat capacity is nearly constant for that temperature change. This allows the temperature of the calorimeter between pulses to be estimated as being linearly dependent on time. The ΔT can be found by extrapolating the linear dependence of the temperature before and after the heat pulse to some intermediate temperature and finding the difference between the two extrapolated lines. [32]

# Chapter 2: Results and Discussion

## *2.1 X-Ray Diffraction*

The X-ray diffraction patterns for the samples showed that the samples were single phase, although some show traces of pure indium. None of the samples shows signs of another R-In intermetallic phase.

Initially, the samples were analyzed using Cu Kα powder X-ray diffraction from 2θ of 20° to 90° but due to the cubic crystal structure, only a few Bragg peaks appeared within this range. The data were then recollected to 120° in an attempt to improve the accuracy of calculation of the lattice parameter. However, even with the extra peaks, Reitveld refinement did not converge to a stable value of the lattice parameters. This was attributed to the fact that the peaks were very broad resulting from deformation and stress introduced the material when it was ground into a powder.

In order to improve the diffraction patterns by removing the stresses, the materials needed to be annealed as powders. The amount of powder needed to obtain a diffraction pattern is fairly small (enough to cover about 1$cm^2$), but when there are over 40 different compositions to be heat treated there needs to be a simple repeatable process. To accomplish this, thin rods of tantalum tubing were cut into segments of about 1 inch in length. One end of each of the tubes was pinched shut and then welded in an argon environment using an arc-welder. The tubes were then outgassed in an induction furnace under vacuum. Each tube was then filled with a different compositional sample that had been ground into a powder using a pestle and

mortar. The open end of the filled tubes were then pinched shut. Finally, the tubes were heat treated at 600°C for 1 hour in the induction furnace under vacuum in two batches: the first with 24 samples and the second with 18.

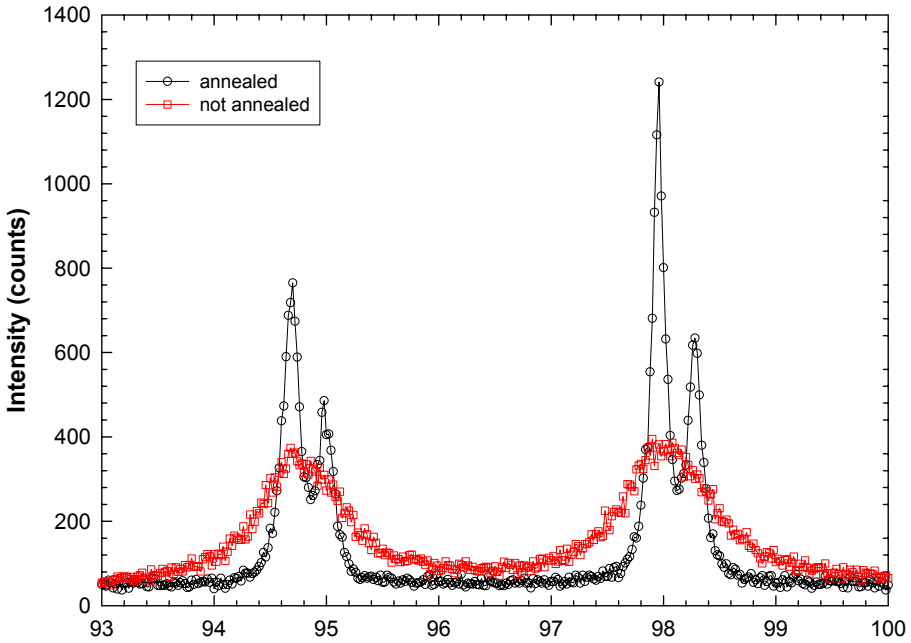


**Figure 2-1: Close up view of two Bragg peaks showing the affect that heat treatment has on the sample $(Ho_{0.6}Er_{0.4})In_3$.**

The results of this heat treatment were striking. The difference in the shapes of two peaks can be seen for $(Ho_{0.6}Er_{0.4})In_3$ in Figure 2-1. In addition, the full width at half maximum, *FWHM*, as a function of 2θ for this sample was modeled using the Cagliotti equation:

$$FWHM = \sqrt{U \tan^2 \theta + V \tan \theta + W}$$

where *U*, *V* and *W* are peak shape parameters that were determined experimentally during refinement [35]. Plotting this function (Figure 2-2) using the parameters found for the annealed $(Ho_{0.6}Er_{0.4})In_3$ vs. the same sample without the annealing shows that the *FWHM* is

smaller for all measured 2θ for the annealed sample. Since the peak width in an X-ray diffraction pattern is dependent on the amount of deformation and stress present in the sample, this shows that annealing the powder removes both.

**Table 2-1: The peak shape parameters determined for the data above using a pseudo-voigt peak shape function.**

| | Annealed | Not annealed |
|---|---|---|
| *U* | 0.021 | 0.50169 |
| *V* | 0.0068 | 0.02192 |
| *W* | 0.016 | 0.00017 |

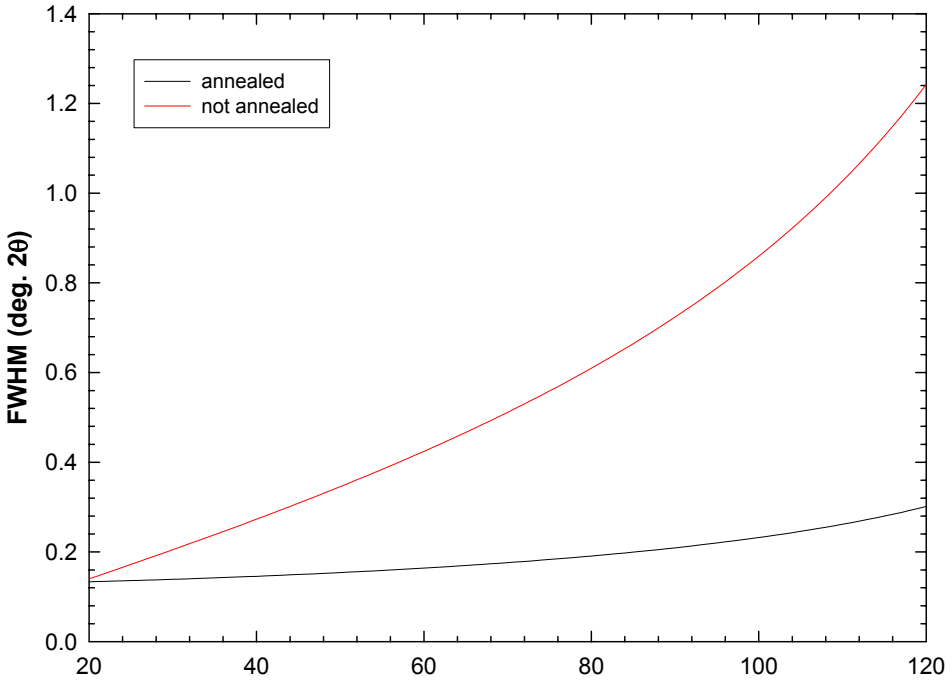


**Figure 2-2: The calculated full width at half maximum as a function of 2θ for $(Ho_{0.6}Er_{0.4})In_3$.**

## *2.2 Heat Capacity*

One point that should be noted about the magnitude of the heat capacity peaks reported here is that for the extremely sharp and narrow peaks, the maximum heat capacity value is not very accurate. While the calorimeter used to obtain the low temperature data collects data quickly and is easy to use, the assumptions made to simplify the measurements break down for rapid changes in the heat capacity with respect to temperature. This occurs because after each heat pulse, the calorimeter waits for the time dependent change in the sample temperature to stabilize. If the heat capacity is sharply changing, then the time dependent temperature will not be linear and can fall outside the acceptable range for what is considered stable. Because of this there will be very few data points during the peak making the accuracy of the heat capacity at those points low. With this said, there still should always be one data point that is at the exact peak temperature due to the heat capacity reaching a maximum and then decreasing. With this inaccuracy, the height of the peak can vary, but theoretically the total heat capacity of the peak (the area under the curve) should be the same for any given sample.

## *2.3 $RIn_3$*

Five $RIn_3$ compounds were prepared with the rare earth elements yttrium, cerium, praseodymium, neodymium and dysprosium. The lattice parameters of these compounds were measured as described above and all found to be within the range of literature values. In addition to this, the magnetic susceptibility of these compounds was also measured. The graphed data and calculated values for these samples were all found using the SQUID

calorimeter because the Lakeshore unit did not have enough sensitivity to provide reliable measurements for the Y, Ce, Pr and Nd compounds due to the small size of their magnetic moments. For the same reason, unless otherwise specified, all the measurements shown used the direct current method of determining the susceptibility.

In determining the magnetic property data for these samples, a region well above the transition was chosen and a linear trend was added as a best fit for that region. This line was then extrapolated to lower temperatures. The Néel temperature was chosen as the temperature at which the data visibly deviated from the linear trend and the Weiss temperature as the temperature at which the linear trend intercepts the temperature axis. The effective magnetic moment of the rare earth elements in the compound was determined using the slope of the linear trend and the relationships described in section 1.1.1.3. Taking the effective magnetic moment of the indium atoms to be zero and noticing that there is exactly one rare earth atom per unit cell allows the rare earth $p_{eff}$ to be calculated using:

$$p_{eff} = \sqrt{\frac{3k_B a^3}{\mu_0 C^{-1}}}$$

where $k_B$ is Boltzmann's constant, $\mu_0$ is the permeability of free space, $a$ is the lattice parameter, and $C^{-1}$ is the inverse of the Curie constant, which is the slope of the linear trend.

The $YIn_3$ compound was measured twice and both times produced similar results showing that the susceptibility remains constant as the temperature changes. This is clearly visible at high temperatures, but at low temperatures, the scatter increases but the susceptibility values are still very small.

$PrIn_3$ was also measured twice using different sized samples with the same field in the SQUID. Although the two plots shown in Figure 2-3 follow the same trend, there is clearly some difference in the slope and magnitude at higher temperatures.

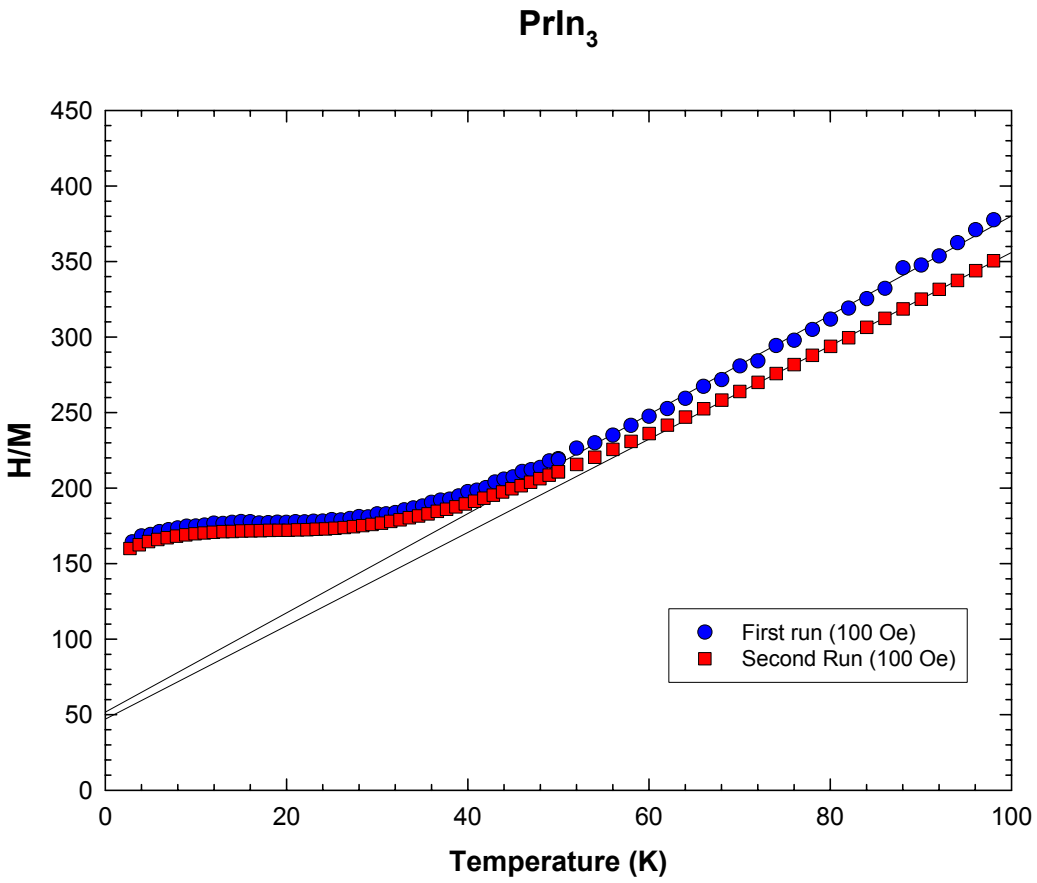


**Figure 2-3: The inverse magnetic susceptibility of $PrIn_3$ measured in a constant magnetic field of 100 Oe. The lines represent the linear trend of the data at higher temperatures. These linear trends were used to calculate the Weiss temperature and the Curie constant.**

The Weiss temperature constant found for both of these lines is found to be -15, (Table 2-2) which does deviate from the literature values of -9 and -10 (Table 1-2). The calculated magnetic moments of 3.45 and 3.55 are also somewhat smaller than those found from the literature of 3.58 and 3.72. However, both of these calculated values are dependent on the

slope of the high temperature region, which in the presented data only goes up to 100 K. Determining this slope is dependent on determining where the data deviate from linearity. For $PrIn_3$, there is no definite temperature at which this occurs and varying the range of points included in the straight line calculation does have a significant effect on the slope of the line.

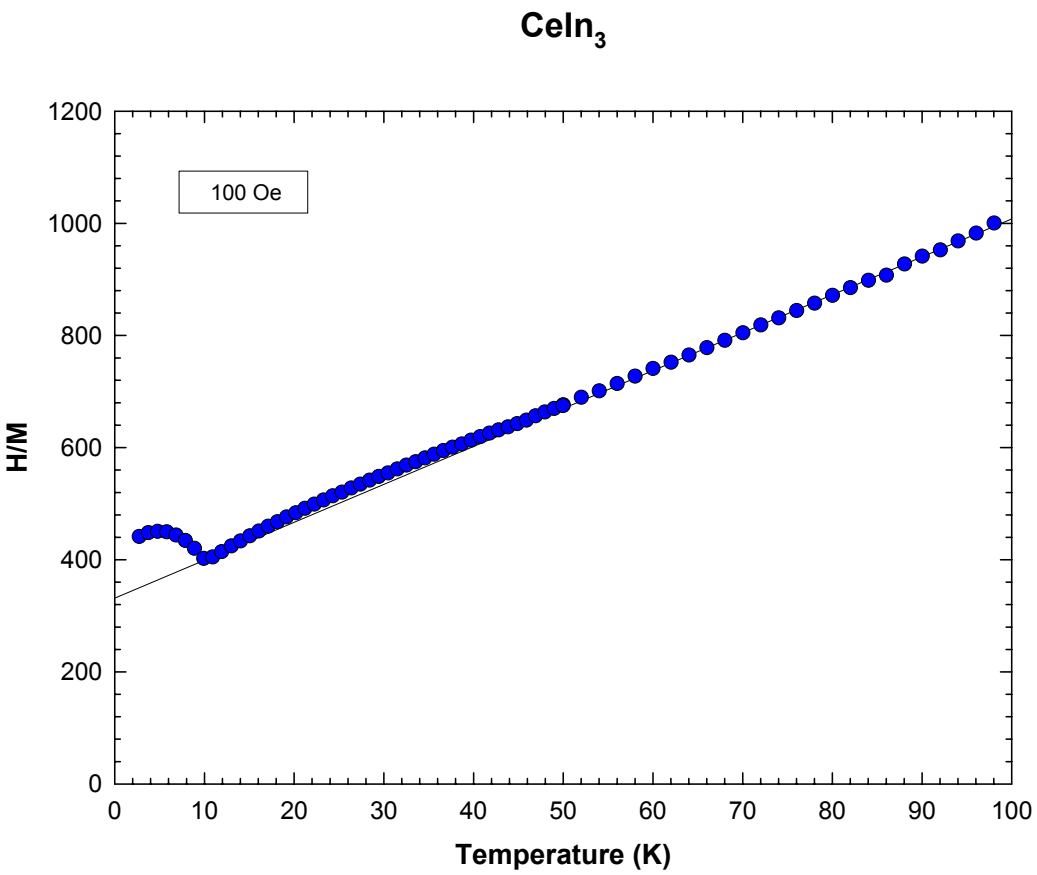


**Figure 2-4: The inverse magnetic susceptibility measured for $CeIn_3$ in a constant magnetic field of 100 Oe. The line represents the linear high temperature trend.**

$CeIn_3$ (Figure 2-4 and Table 2-2) shows a slight divergence around 50 K and also a transformation at 10 K, both of which are consistent with the literature. $NdIn_3$ and $DyIn_3$

(Figures 2-5 and 2-6 and Table 2-2) both show linear high temperature slopes and single transformations at 6 K and 21 K, respectively.

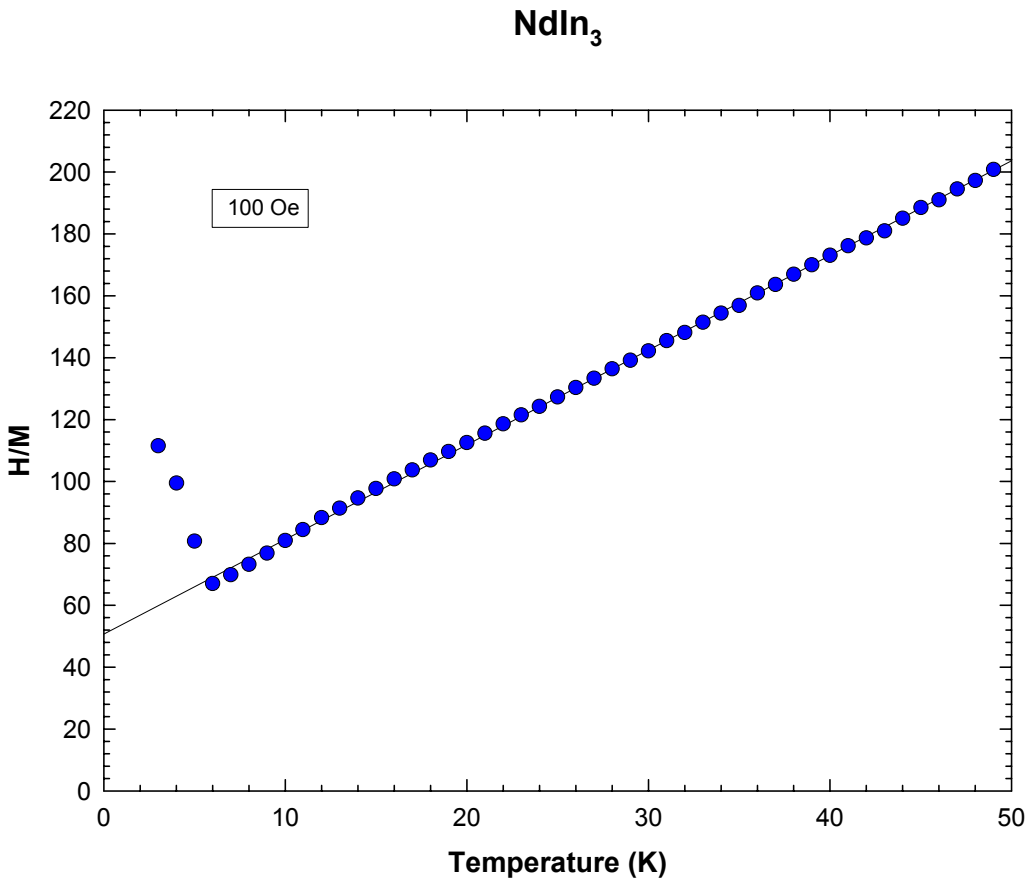


**Figure 2-5: The inverse magnetic susceptibility measured for NdIn3 in a constant magnetic field of 100 Oe. The line represents the linear high temperature trend.**

The theoretical $p_{eff}$ for the rare earth atoms in these compounds is also shown in Table 2-2. The measured values are all within 5% of the calculated values showing a decent agreement between the two. This suggests that the effective magnetic moments of the rare earth atoms in the compounds is essentially the same as the corresponding free atoms.

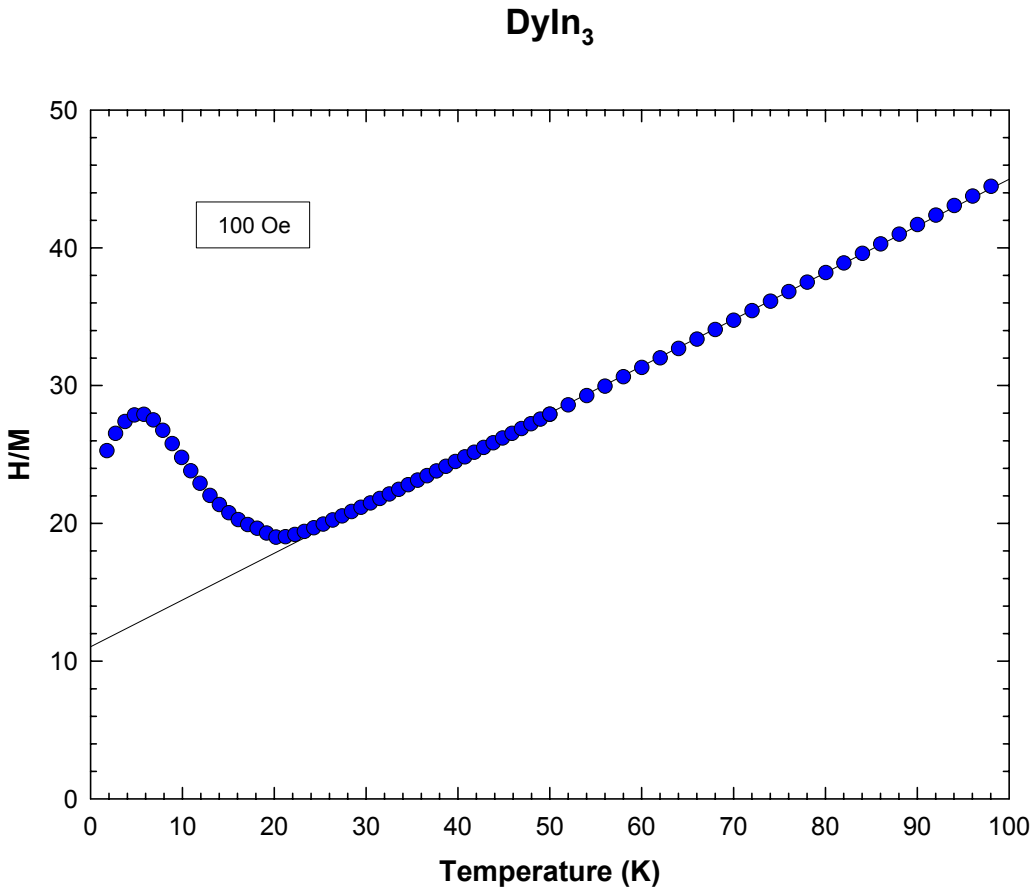


**Figure 2-6: The inverse magnetic susceptibility measured for DyIn3 in a constant magnetic field of 100 Oe. The line represents the linear high temperature trend.**

**Table 2-2: The crystallographic and magnetic property data of the $RIn_3$ compounds. The theoretical effective magnetic moments were determined using the equations given in section 1.1.2.3.**

| Compound | $a$ (Å) | $\theta_C$ (K) | $T_N$ (K) | $p_{eff}$ ($\mu_B$) | Theoretical $p_{eff}$ ($\mu_B$) |
|---|---|---|---|---|---|
| $YIn_3$ | 4.5926 | | | | |
| $CeIn_3$ | 4.6894 | -49 | 10 | 2.42 | 2.54 |
| $PrIn_3$ | 4.6717 | -15, -16 | | 3.45, 3.55 | 3.58 |
| $NdIn_3$ | 4.6554 | -17 | 6 | 3.56 | 3.62 |
| $DyIn_3$ | 4.5806 | -33 | 21 | 10.4 | 10.63 |

## *2.4 $ErIn_{3\pm x}$*

The differences in the reported values for the heat capacity peak of $ErIn_3$ suggest that there might be a solid solubility range around the ideal stoichiometric composition. To determine if this is true, an indium-rich sample, $ErIn_{3.2}$, and an indium-deficient sample, $ErIn_{2.9}$, were prepared. The lattice parameters for these samples were calculated from X-ray diffraction patterns of the samples. The results are shown in Table 2-3 along with the lattice parameters calculated for $ErIn_3$.

**Table 2-3: The calculated lattice parameters and magnetic ordering temperatures (from heat capacity measurement) for the $ErIn_{3\pm x}$ compounds.**

| Compound | $a$ (Å) | $T_N$ (K) | Source |
|---|---|---|---|
| $ErIn_3$ | 4.5658 | | this work |
| | 4.5667 | 4.4 | [29] |
| $ErIn_{2.9}$ | 4.5662 | 4.4 | this work |
| $ErIn_{3.2}$ | 4.5657 | 4.9 | this work |

There is a slight downward trend in the lattice parameters for the samples calculated in this work as the indium content increases. This suggests that the lattice parameter might decrease as the indium content increases, as should be expected if indium is substituting on erbium sites. However, it should be noted that the variation in lattice parameters determined for these three compounds is smaller than the variation between the previously reported value for $ErIn_3$ and the recalculated value from the exact same sample.

The heat capacity of $ErIn_{3.2}$ was shown to have a narrow sharp peak at 4.9 K while $ErIn_{2.9}$ exhibits a lower, broader peak at 4.5 K (Figure 2-7). These two different peaks seem to

confirm that the difference between the literature heat capacity data for $ErIn_3$ is real, and is the result of the amount of indium in the samples.

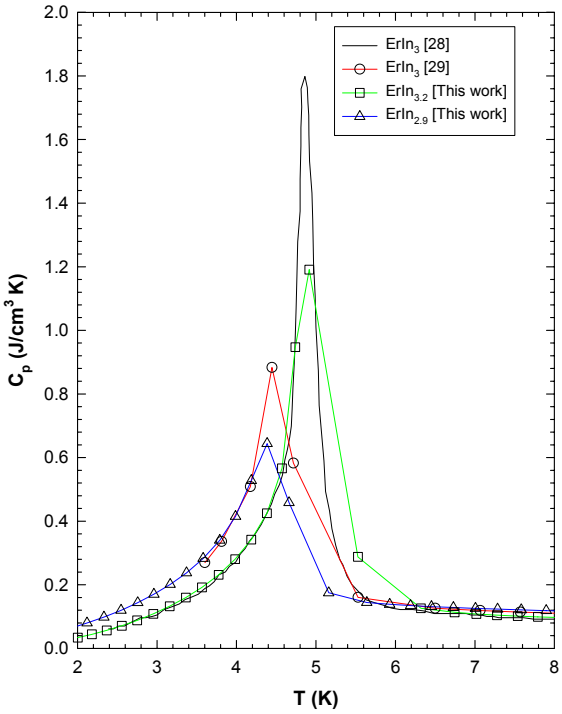


**Figure 2-7: The low temperature heat capacity peaks of $ErIn_{3.2}$ and $ErIn_{2.9}$ compounds.**

To test whether $HoIn_3$ also behaves this way, $HoIn_{3.1}$ was also prepared and studied. Both the lattice parameter and the heat capacity of $HoIn_{3.1}$ were found to be almost identical to $HoIn_3$. This suggests that varying the indium concentration in $HoIn_3$ does not affect its properties although an indium deficient sample needs to be studied to confirm this.

**Table 2-4: The calculated lattice parameters for the $HoIn_{3+x}$ compounds.**

| Compound | *a* (Å) | Source |
|---|---|---|
| $HoIn_3$ | 4.5734 | this work |
| | 4.5731 | [29] |
| $HoIn_{3.1}$ | 4.5731 | this work |

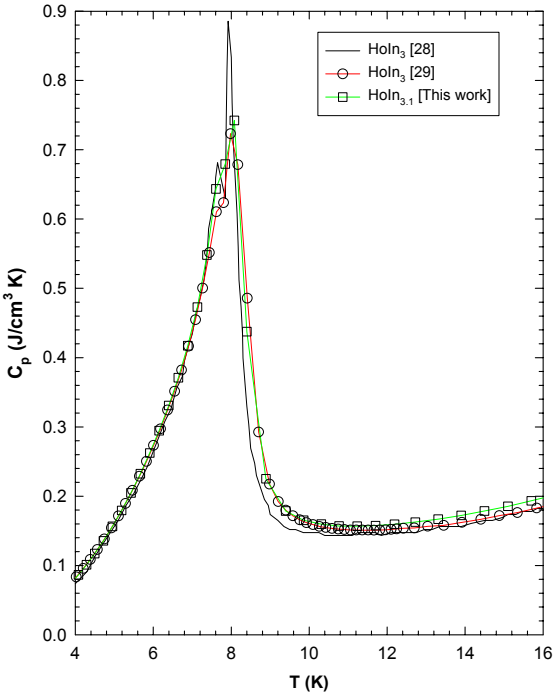


**Figure 2-8: The low temperature heat capacity peak of $HoIn_{3.1}$ shown on relation to $HoIn_3$.**

## *2.5 $(Ho_xEr_{1-x})In_3$*

The lattice parameters for the $(Ho_xEr_{1-x})In_3$ compounds that were reported by Gschneidner, et al. [29] were recalculated using the procedure described above. This was done for a number of reasons. The samples were on hand, making retesting a trivial task. Also, the reported lattice parameters came from diffraction data using Mo Kα radiation from 9 to 50 degrees 2θ. Thus, recalculating the lattice parameters allows for a consistency check between the two methods and within the same sample. In addition, the experimental procedure for the lattice parameter refinement for these samples would be consistent with the new samples that were prepared for this work. Finally, it was hoped that the new procedure would produce a result

with a higher accuracy. The recalculated lattice parameters are shown together with the reported values in Figure 2-9.

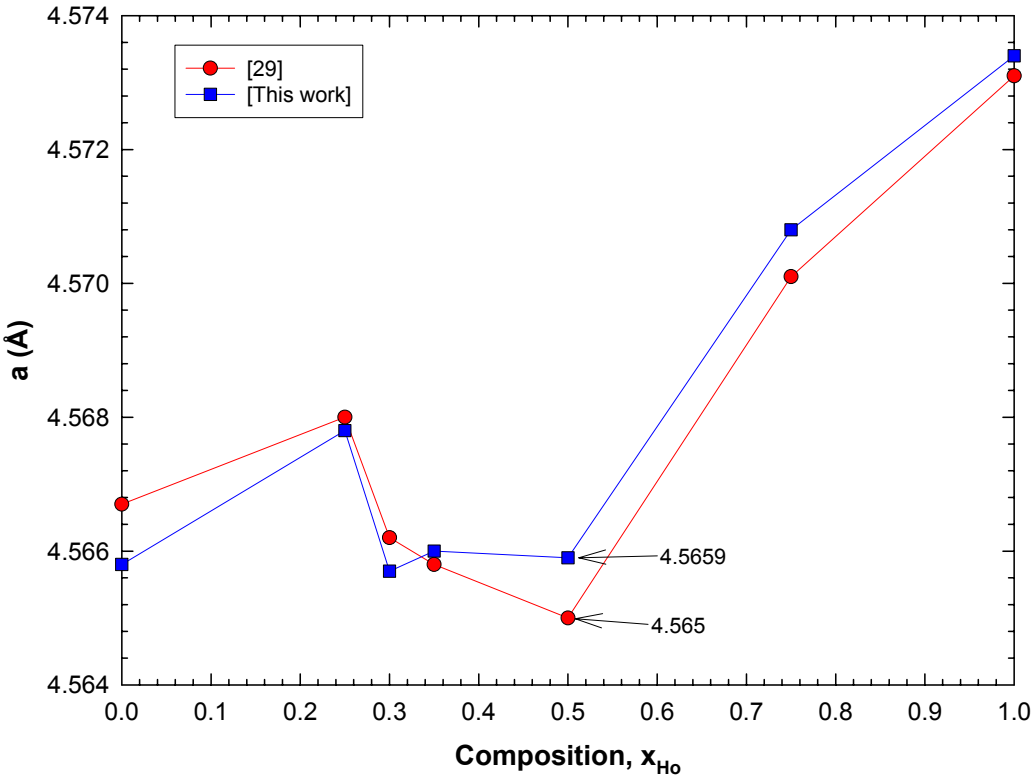


**Figure 2-9: A comparison of the lattice parameters reported [29] and the recalculated values from the same samples.**

The largest difference between the calculated lattice parameters for each sample was 0.0009 Å for $ErIn_3$ and $Ho_{0.5}Er_{0.5}In_3$ showing that the two measurement techniques agree well and confirming that for the x = 0.3, 0.35 and 0.5 samples, the lattice parameters do not follow the linear trend with the rest of the samples and their new lattice parameter values are closer to each other. A linear change from $ErIn_3$ to $HoIn_3$ is indeed expected from Vegard's Law,

which should be valid for this system. The recalculated values also show that the lattice parameter of $ErIn_3$ is closer to the literature values.

In addition to reexamining the old samples, 15 new samples were prepared across the $(Ho_xEr_{1-x})In_3$ family of compounds and were made in three separate batches. The first group included the values x = 0.275, 0.4, 0.6, 0.7, and 0.85 and attempted to refine the dip that was shown by Gschneidner, et al. [29]. After making the samples, it was noticed that there was an error in the weighing of the $(Ho_{0.7}Er_{0.3})In_3$ sample, and the actual weighed composition was $(Ho_{0.7}Er_{0.3})In_{3.01}$.

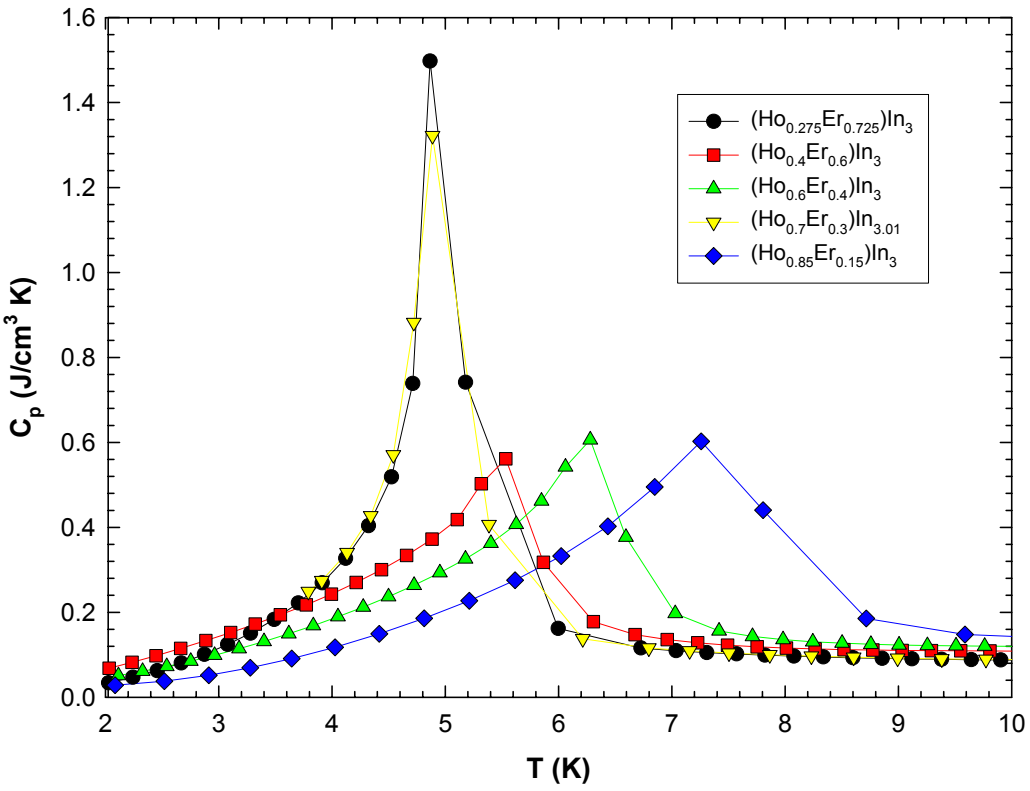


**Figure 2-10: The low temperature heat capacities of the first batch of new $(Ho_xEr_{1-x})In_3$ alloys.**

The heat capacity measurements for these samples are shown in Figure 2-10. The $(Ho_{0.275}Er_{0.725})In_3$ and $(Ho_{0.7}Er_{0.3})In_{3.01}$ samples had narrow sharp peaks at 4.87 and 4.89 K with maximum heat capacities of 1.50 and 1.32 J/cm$^3$ K respectively. The other three samples, x = 0.4, 0.6 and 0.85, had lower and broader peaks at 5.5, 6.3 and 7.3 K with heat capacity maximums of 0.56 , 0.61, and 0.60 J/cm$^3$ K respectively. When the Néel temperatures of these samples are plotted together with the previously determined values by Gschneidner, et al. [29] (Figure 1-7), the dip in the data is replaced by two linear trends (Figure 2-11). One trend follows the simple linear change of $T_N$ from $ErIn_3$ to $HoIn_3$ across the compositions according to Vegard's law. The other linear trend keeps the Néel temperatures of the samples near 4.9 K regardless of the composition.

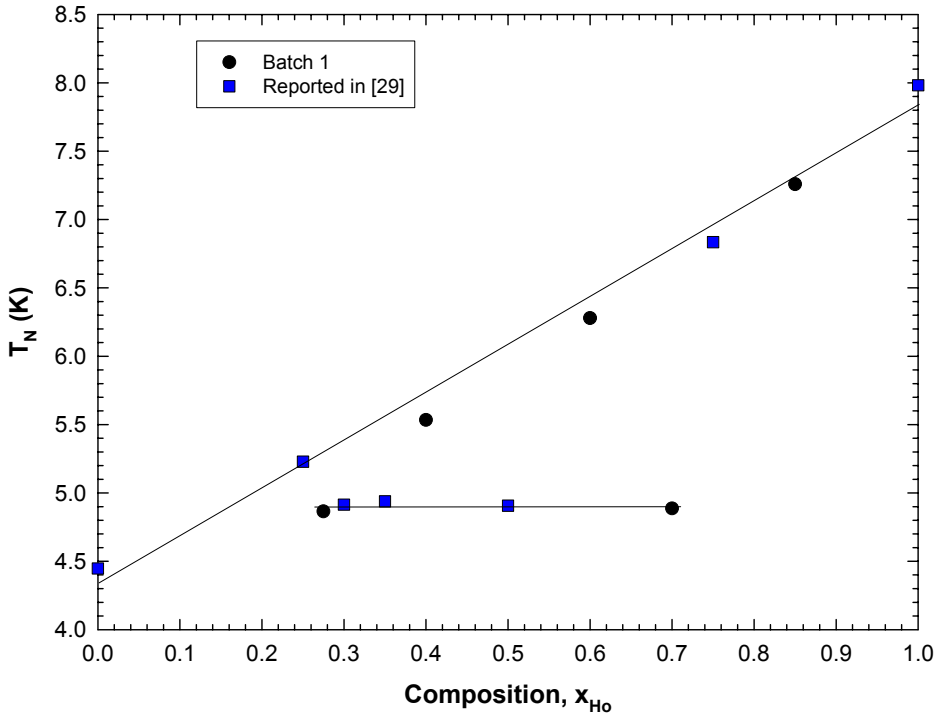


**Figure 2-11: The Néel temperatures for the first batch of new compounds with those reported in [29]. The two lines are drawn to emphasize what appears to be two different trends.**

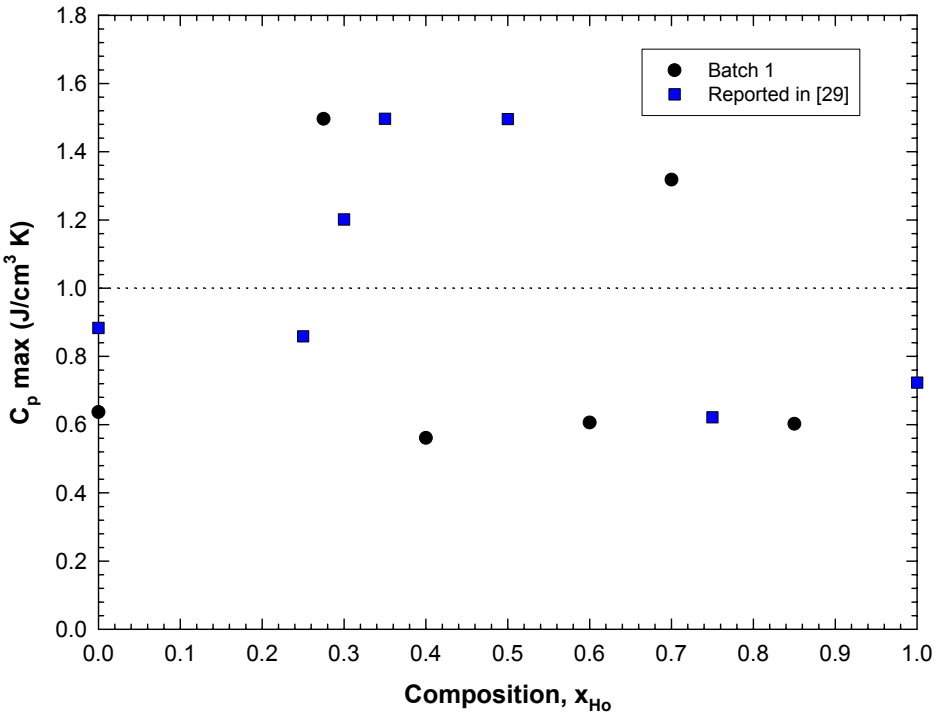


**Figure 2-12: The maximum heat capacity peaks plotted as a function of composition for the first twelve compounds. The data points below the line correspond to the Vegard's law trend seen in Figure 2-11, while those above the line correspond to the other linear trend in that figure.**

It is also interesting to note the relationship between the maximum heat capacity (Figure 2-12) and the peak temperatures. All of the samples that have Néel temperatures at 4.9 K have maximum heat capacity values greater than 1 J/cm$^3$K while all the rest are below this. In fact, the maximum heat capacity of the 4.9 K samples is nearly twice what it is for the others.

The lattice parameters of these samples were also calculated and included with the recalculated lattice parameters for the original compounds (Figure 2-13). This plot is very similar in appearance to Figure 2-11 in that there appear to be two trends: one following Vegard's law and the other independent of composition.

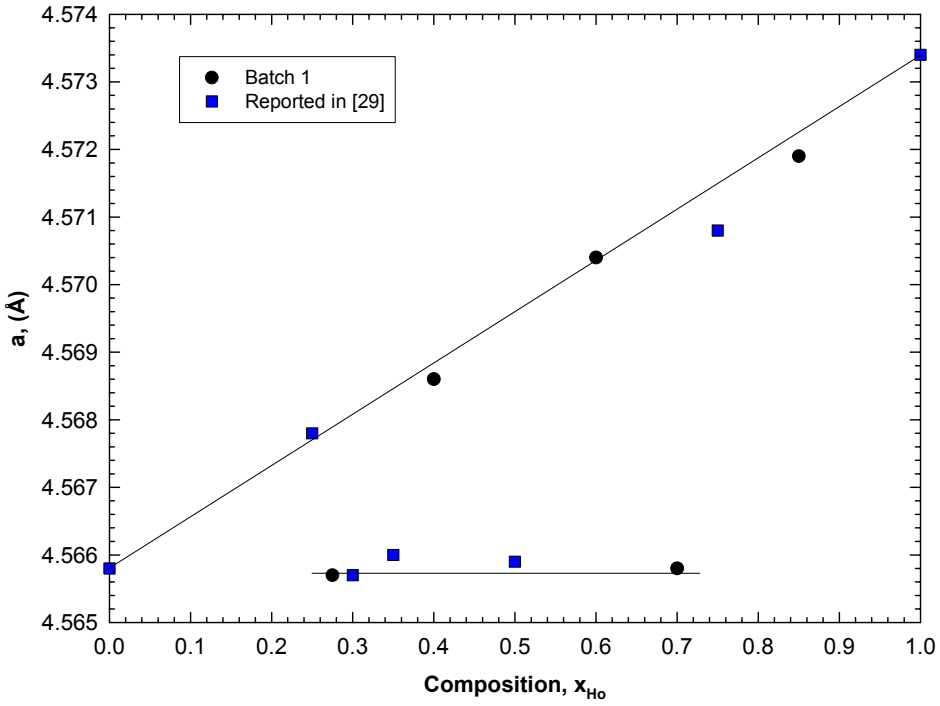


**Figure 2-13: The lattice parameter values as a function of composition for the first twelve compounds. Notice how the dipping trend seen in Figure 2-9 is now replaced with what appears to be two separate linear trends. Also note the similarity between this figure and Figure 2-11.**

Following this, a second batch of alloys was prepared to investigate the anomalous 4.9 K trend. Six new samples were prepared with x = 0.29, 0.31, 0.49, 0.51, 0.69 and 0.71 to compare with the already existing samples with x = 0.3, 0.5 and 0.7. All of these newer samples have lattice parameters and heat capacity peaks that are characteristic of the linear trend between $ErIn_3$ and $HoIn_3$ instead of the 4.9 K trend. The differences in the heat capacities of these six samples when compared to the three previous ones of similar compositions are striking and can be seen in Figure 2-14.

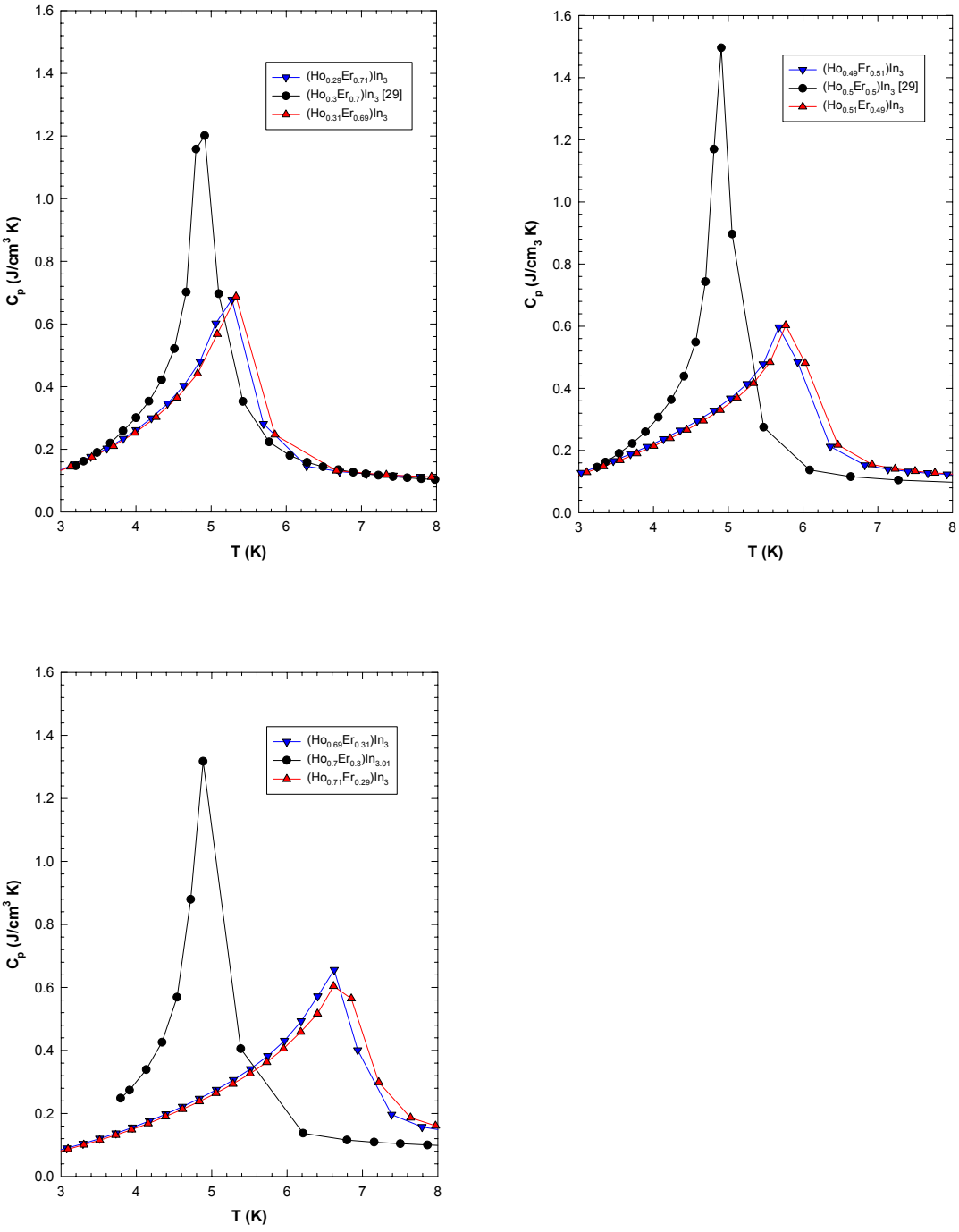


**Figure 2-14: The low temperature heat capacity comparing three of the anomalous samples to similar compounds.**

The second batch of six samples indicate that the anomalous 4.9 K $T_N$ points are not due to changes in the rare earth content and must be the result of some other factor. It was noticed that the anomalous heat capacity peaks are almost identical to the heat capacity peak for $ErIn_{3.2}$ as shown in Figure 2-7. In addition to this and the fact that $(Ho_{0.7}Er_{0.3})In_{3.01}$ is known to have a slight excess of indium, it was thought that the indium content of the samples could be the cause of the change in heat capacity properties. Because of this, a third batch of samples was prepared to test this hypothesis by preparing $(Ho_{0.12}Er_{0.88})In_{2.9}$ and three $(Ho_xEr_{1-x})In_{3.1}$ samples with x = 0.12, 0.4 and 0.85.

The x = 0.12 samples showed that the indium-rich sample has a heat capacity peak at 4.9 K, while the indium-deficient sample has a peak at 4.6 K. The lattice parameter for $(Ho_{0.12}Er_{0.88})In_{3.1}$ was found to be 4.5666 Å, while the lattice parameter for $(Ho_{0.12}Er_{0.88})In_{2.9}$ was found to be 4.5672 Å. This means that the lattice parameter for $(Ho_{0.12}Er_{0.88})In_{3.1}$ is slightly closer to the lattice parameter of $(Ho_{0.12}Er_{0.88})In_{2.9}$ than it is to the other samples with heat capacity peaks at 4.9 K (~4.559Å), although the difference in either direction is within experimental error. This seems to confirm that at least for small amounts of holmium, the indium concentration does affect properties.

The indium rich x = 0.85 sample resulted in lattice parameter and heat capacity data (Figure 2-14) almost identical to the sample that did not contain excess indium, which was not entirely unexpected based on the results for $HoIn_3$ and $HoIn_{3.1}$. Similarly, the properties measured for $(Ho_{0.4}Er_{0.6})In_{3.1}$ also were almost identical to those measured for $(Ho_{0.4}Er_{0.6})In_3$. These results are show below in Figure 2-14.

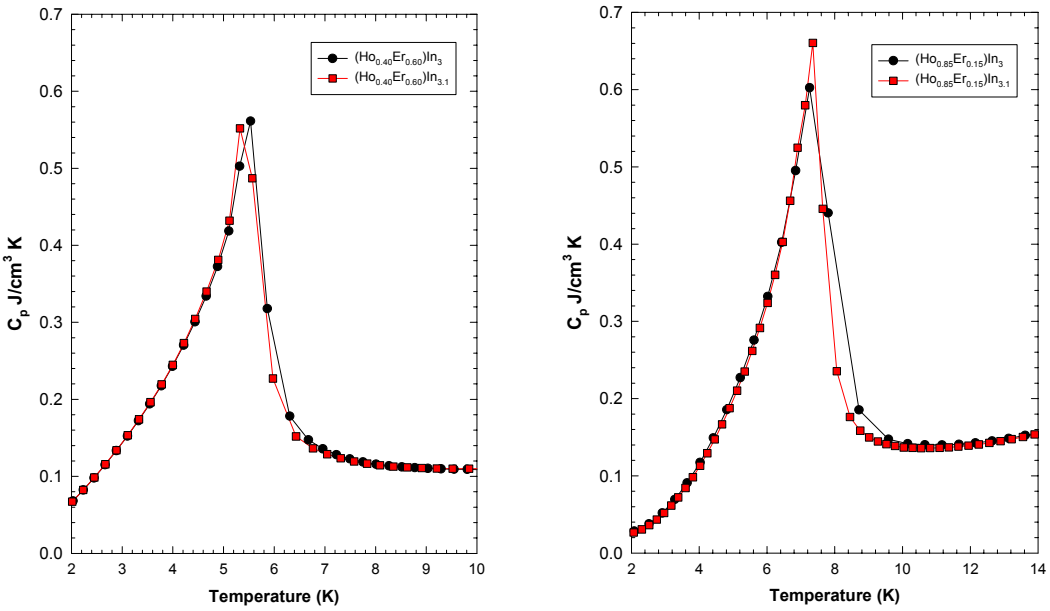


**Figure 2-14: A comparison of the low temperature heat capacities between $(Ho_xEr_{1-x})In_3$ and $(Ho_xEr_{1-x})In_{3.1}$ for x = 0.4 and 0.85.**

The Néel temperatures, maximum heat capacities and lattice parameters determined for all of the $(Ho_xEr_{1-x})In_{3\pm y}$ compounds are shown in Figures 2-15, 2-16 and 2-17 respectively. The similarity between the plot of $T_N$ values and the plot of lattice parameters is striking. The samples that have $T_N$ values near 4.9 K all have similar lattice parameters, while the rest of the data points seem to follow Vegard's law for both. The maximum heat capacity values show a wide range and scatter that is due to the fact that the assumptions made for the heat capacity measurement technique suffer during large sudden changes in the heat capacity. The actual magnitude values shown are not that accurate, but it is enough to note that all of the peaks with maximum heat capacity values greater than 1.0 J/cm$^3$ K have a $T_N$ near 4.9K.

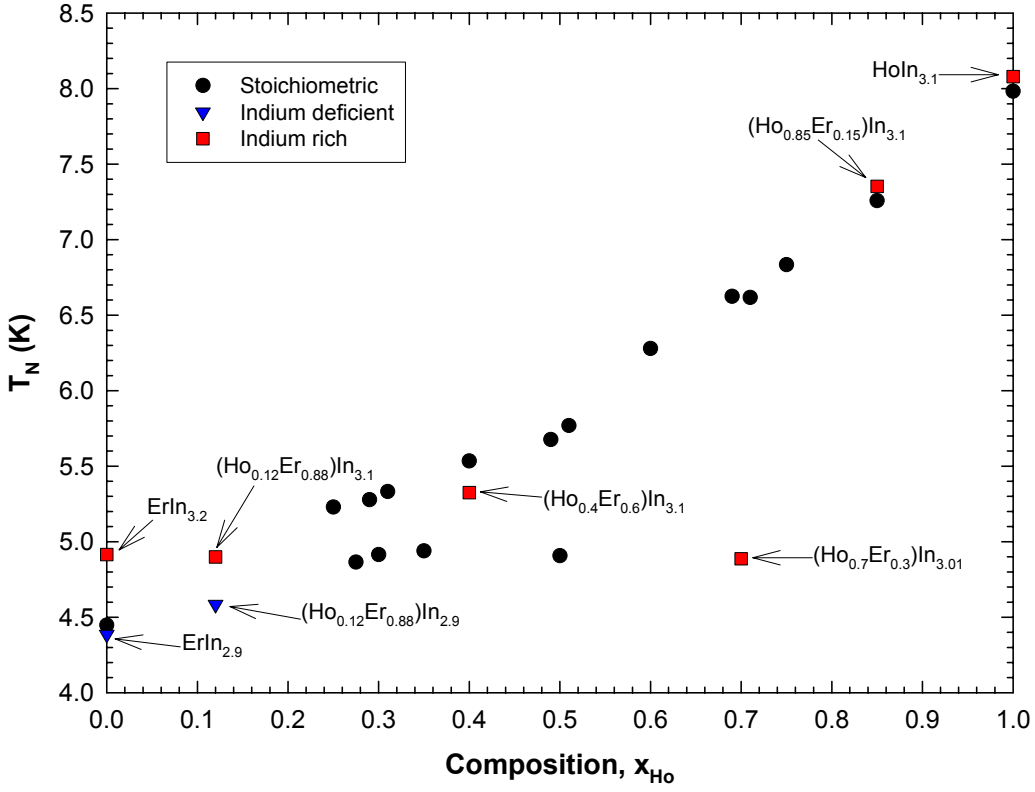


**Figure 2-15: The Néel temperatures found by calorimetry for all of the $(Ho_xEr_{1-x})In_{3\pm y}$ compounds. The values corresponding to the $y \neq 0$ samples are labeled.**

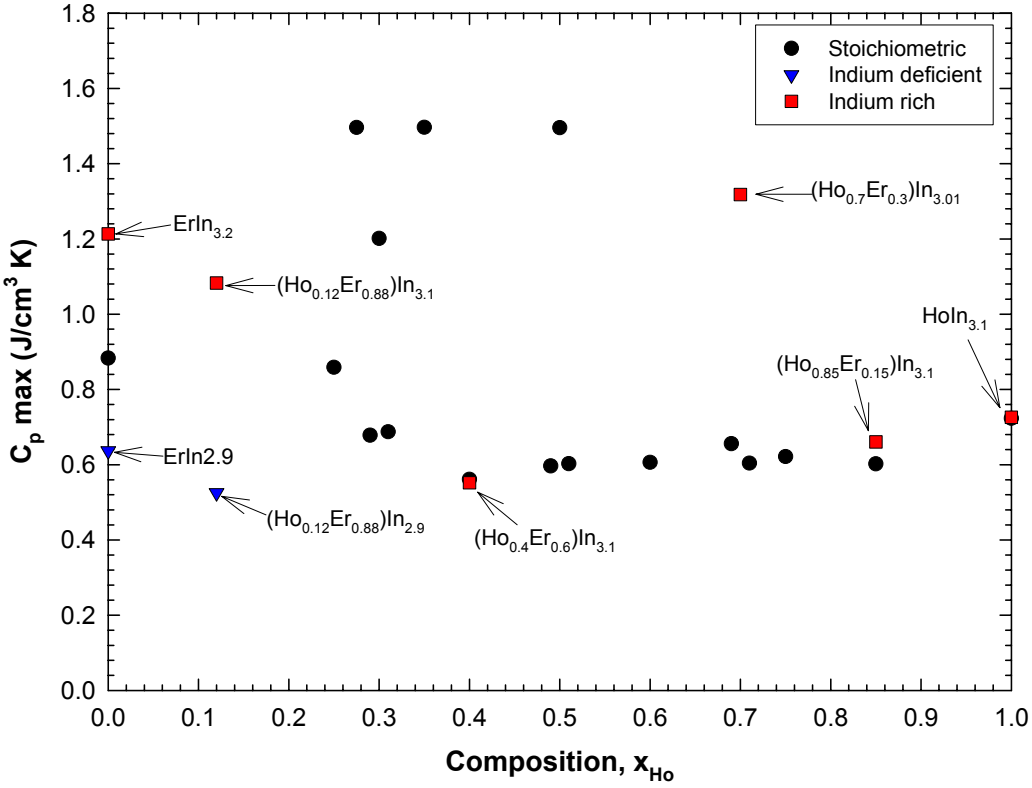


**Figure 2-16: The maximum heat capacity for all of the $(Ho_xEr_{1-x})In_{3\pm y}$ compounds. The values corresponding to the $y \neq 0$ samples are labeled.**

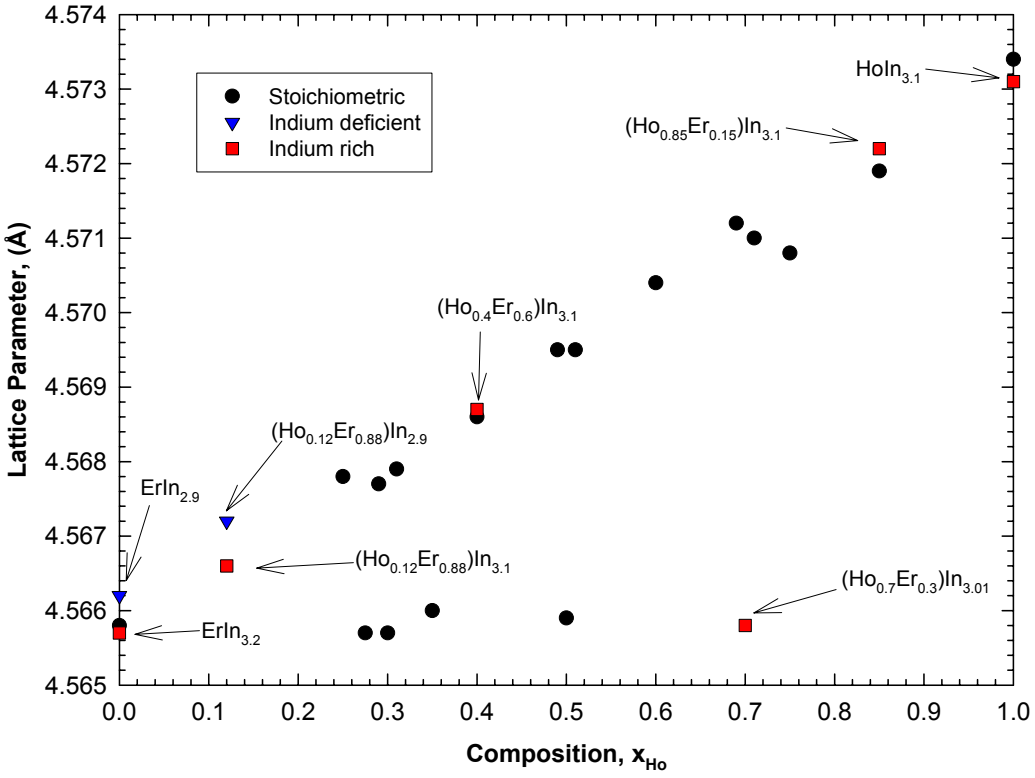


**Figure 2-17: The calculated lattice parameters for all of the $(Ho_xEr_{1-x})In_{3\pm y}$ compounds. The compounds where $y \neq 0$ are labeled. Note the similarity in the apperance between this figure and Figure 2-15.**

The indium rich 0.4 sample seems to disprove the fact that the anomalous data are the result of varying compositions of indium. This results in a lack of an explanation for why some of the samples have the 4.9 K peaks instead of following the linear trend. Some possible explanations could be that there is another chemical impurity that is causing these results which is not detected in the XRD patterns. If the indium content can have a large effect on the heat capacity of $ErIn_3$ it is possible that another impurity can also be affecting these samples.

The results also suggest another possibility: the anomalous data could in fact be all samples that are $ErIn_3$ with no holmium because the metal added to make the $(Ho_xEr_{1-x})In_3$ alloy was not holmium as expected, but was in fact erbium by mistake. While this might be a possibility, it seems unlikely because the anomalous data showed up in four different batches of samples prepared over three years and from two different sources of holmium. In either case, if there are unseen impurities or the samples are not what they should be, the only way of telling is performing a chemical analysis which should be done on these samples if this research is continued.

A third possibility is that those alloys that do not follow Vegard's law are not perfectly ordered. The $AuCu_3$-type crystal structure that the $RIn_3$ compounds have appears to be face-centered cubic, but the ordered arrangement of the two constituent atoms actually makes the structure simple cubic. The XRD patterns of the ordered simple cubic structure will contain certain peaks that are forbidden for the disordered face-centered cubic structure. These peaks are known as superlattice reflections. A variation in the relative intensity of the superlattice peaks across the samples would be indicative of a variation in the amount of ordering. A quick glance at the XRD patterns for the samples presented in this paper showed no clear distinction in the superlattice reflections between the two trends of samples. Thus, if there is a difference in the amount of ordering, it is not apparent in the bulk samples although small disordered regions could still be present. If this is the case, it should be possible to remedy the ordering discrepancy by heat treating the sample near its melting point, or by melting the sample again.

## *2.6 $(R_xEr_{1-x})In_3$*

The low temperature heat capacities were also measured for eight samples containing combinations of erbium and another rare earth element besides holmium. These eight samples were of the compositions $(R_{0.05}Er_{0.95})In_3$ and $(R_{0.1}Er_{0.9})In_3$ for R being yttrium, cerium, praseodymium and dysprosium. Because of this, it is probably more apt to describe these samples as being mostly $ErIn_3$ with slight additions of the other rare earth elements.

The lattice parameters for these samples have been calculated as described above using powders that have been heat treated. The results of these measurements are plotted in Figure 2-18 with linear trend lines between the calculated lattice parameter for $ErIn_3$ and the lattice parameters for the corresponding $RIn_3$ samples that were mentioned earlier (see section 1.1.1.2 and Table 1-1.) The lattice parameters for these mixed samples all fall on or near the expected linear trend lines.

As for the effect of the additions on the heat capacity properties, the four different rare earth elements had different results. It was found that adding cerium (Figure 2-19b) or praseodymium (Figure 2-19c) to $ErIn_3$ results in lowering both temperature and magnitude of the heat capacity peaks with the cerium additions being more effective than the praseodymium additions.

The samples containing yttrium (Figure 2-19a) show interesting behavior in that $(Y_{0.05}Er_{0.95})In_3$ has a higher Néel temperature and peak height than $ErIn_3$ while $(Y_{0.1}Er_{0.9})In_3$

has a lower temperature and peak height. The difference between these three peaks is much less profound than for the other $(R_xEr_{1-x})In_3$ systems.

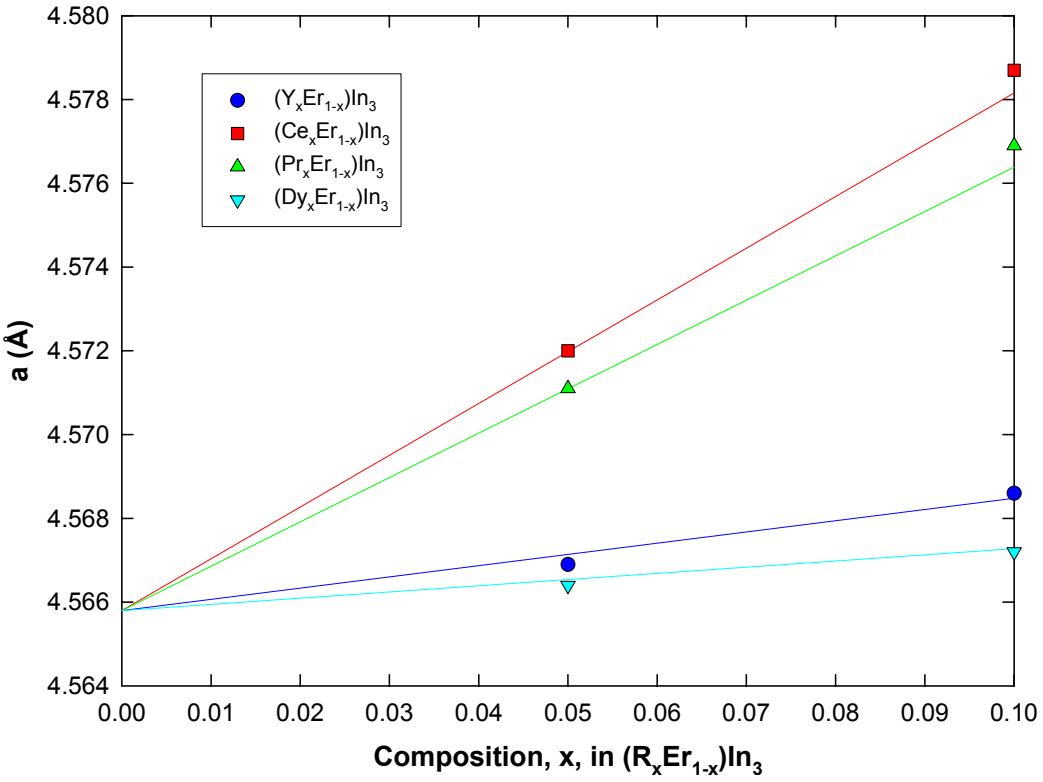


**Figure 2-18: The lattice parameters for eight $(R_xEr_{1-x})In_3$ alloys. The lines correspond to Vegard's law connecting the lattice parameter of $ErIn_3$ to the lattice parameters of the $RIn_3$ compounds.**

Adding dysprosium, (Figure 2-19d) increases the Néel temperature of the compounds while keeping the maximum peak height fairly large. In this way, the $(Dy_xEr_{1-x})In_3$ system behaves much like the $(Ho_xEr_{1-x})In_3$ system, but the dysprosium additions have a greater effect on the transition temperature than a similar addition of holmium. For example, the $(Dy_{0.1}Er_{0.9})In_3$ compound has a peak temperature and magnitude similar to the $(Ho_{0.51}Er_{0.49})In_3$ compound.

Because of this, the $(Dy_xEr_{1-x})In_3$ system could also be studied for its potential as a regenerator material.

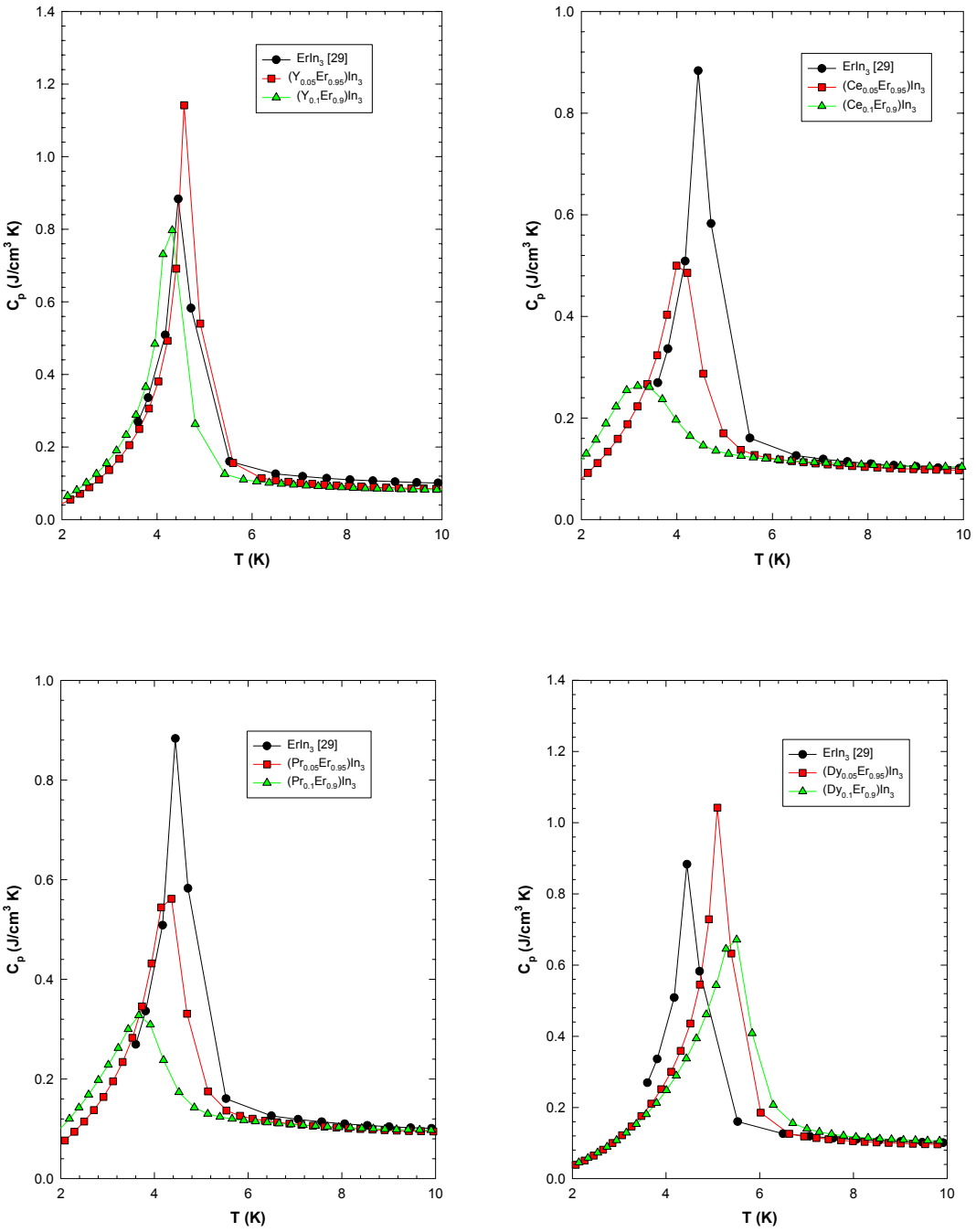


**Figure 2-19: The low temperature heat capacities for the $(R_xEr_{1-x})In_3$ compounds in comparison to $ErIn_3$. R = Y for (a), Ce for (b), Pr for (c) and Dy for (d).**

## *2.7 $ErIn_3$ Powder*

While preparing powders of the $ErIn_3$ alloy for the XRD using an agate mortar and pestle, it was noticed that the material is not very brittle. When struck, the surface of the ingot will deform slightly before the sample will crack. This led to an attempt to prepare tensile test samples of $ErIn_3$. The test samples were prepared by arc-melting a bulk circular ingot into thin fingers and then machining the middle of the fingers into cylinders. Two of the four fingers broke during machining and the other two cracked just after loading into the test apparatus. From this, it was determined that $ErIn_3$ is too brittle to be measured in this manner. Although no quantitative results came from this, it seems necessary to mention this in light of some of the other results.

As previously described, obtaining the lattice parameters of the samples reported on in this study was rather challenging. When the compounds were ground in the preparation of powder diffraction samples, the act of grinding seems to have been enough to plastically deform the compounds. Because of this, the powders had to be heat treated to remove the deformation and obtain good lattice parameter values.

While this may seem trivial at first, it is very important because one of the cheaper ways of using $ErIn_3$ as a regenerator matrix material is by grinding it into a powder with particles within a specific size range. If the $ErIn_3$ particles accumulate large defect densities when it is ground to a powder, it is very likely that this will affect other properties such as the heat capacity. In fact, further results show that this does greatly change the heat capacity properties.

Additional $ErIn_3$ samples were prepared by using commercial erbium. The weight measurement of the commercial erbium before melting was not corrected for the oxygen and carbon impurity contents resulting in the actual erbium content being slightly lower than stoichiometric (thus these samples contain excess indium). The samples were then crushed and ground and metal sieves were used to separate out powder that was between 180 to 300 μm in diameter.

In collaboration with Juraci Sampaio, a portion of the powder was compressed into a pellet using silver binder. The low temperature heat capacity of this sample had a low, broad peak around 5.3 K. This peak is shown in Figure 2-20 along with the peaks of the bulk samples that were previously mentioned. It was first thought that this change in the heat capacity was due to the silver binder holding the powder together, but the results were the same for $ErIn_3$ powder that was compressed without using the silver binder.

Next, the powder was heat treated to 600°C for 1 hour, and the heat capacity was retested, and it was found that the heat capacity peak changed to 4.9 K with a maximum heat capacity even larger than the bulk samples. Since these samples were not corrected for their indium content and thus are indium rich, it is consistent that the $T_N$ for the annealed powder is the same as the $T_N$ for the $ErIn_{3.2}$ sample. The lattice parameter calculated from this annealed powder of commercial $ErIn_3$ was found to be 4.5660 Å, which is nearly the same as the values reported for the pure samples in section 2.4.

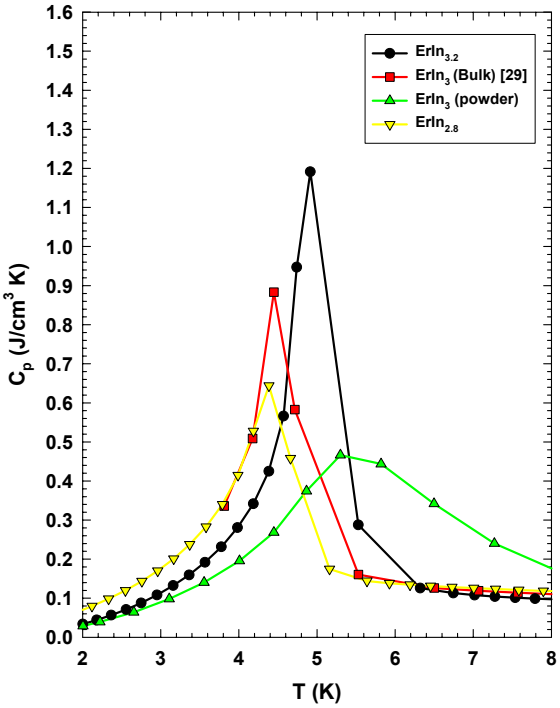


**Figure 2-20: The low temperature heat capacity of $ErIn_3$ powder shown in comparison to the bulk samples. The powder used was made using commercial erbium and should be slightly indium rich. The powder was pressed into a pellet using silver as a binder.**

Following the heat treatment, the powder was once more compressed, and the heat capacity of the pressed pellet was measured. This resulted in a short, broad peak similar to the peak after the first deformation. Finally, the pressed sample was once again heat treated at 600°C and measured resulting in a reemergence of the 4.9 K Néel temperature. The results of these tests are visible in Figure 2-21.

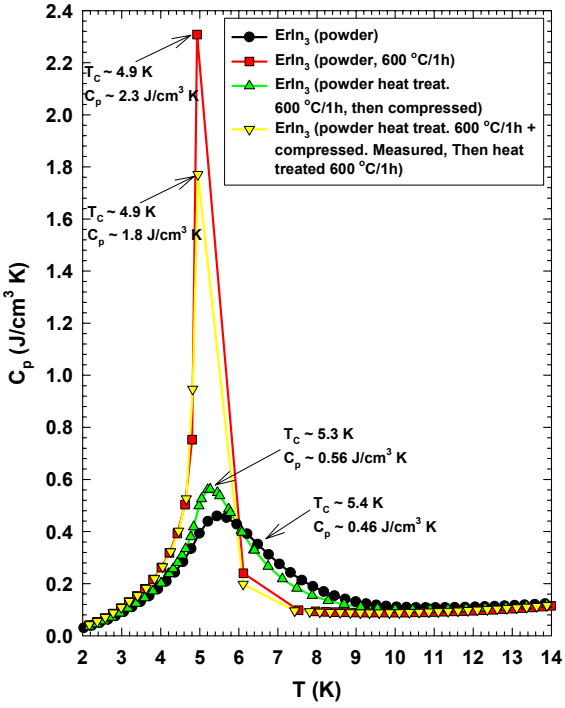


**Figure 2-21: The effect of physical deformation and heat treatment on the heat capacity peak of $ErIn_3$.**

From all of this, we conclude that the slight physical deformation that was identified visually and from X-ray diffraction has a drastic effect on heat capacity. By crushing $ErIn_3$ into a powder, defects are introduced into the crystalline lattice that seem to broaden the range over which the material undergoes its magnetic transformation, resulting in a low, broad peak instead of a narrow, sharp peak. This deformation has been shown to be removed by heat treating the powder.

## *2.8 Induction Melted Sample*

Samples of $ErIn_3$ were also prepared using an induction furnace. A 25 gram sample was made by mixing stoichiometric parts of pure indium and MPC-quality erbium. The erbium and indium were placed inside a tantalum tube that had been out gassed and was welded shut in an argon atmosphere. The tube was then placed inside an induction furnace under vacuum and heated to 1200°C for 1 hour. After cooling, the tube was cut open to determine if the sample had reacted with the tantalum. No reaction layer was present, and after removing both ends of the tube, the sample fell out easily. XRD analysis also showed that no tantalum was present in the sample. However, the surface appearance of the sample suggested that the sample was not homogeneously mixed. A second X-ray diffraction pattern was taken for a different region of the same sample. There was a variation in the appearance of the $ErIn_3$ peaks and the size of the pure indium peaks between the two X-ray measurements indicative of the inhomogeneity.

The same sample was then sealed inside a new tantalum tube and reheated to 1550°C for 10 minutes. The temperature was then dropped and held at 1350°C for 30 minutes before cooling. Once the sample had cooled, it was flipped over and heated to 1350°C for another 30 minutes. Following this, the sample still had not reacted with the tantalum, but it also was not homogeneous. Finally, the $ErIn_3$ sample was melted one last time in the induction furnace, but this time it was placed inside an alumina crucible. The sample was placed inside the induction furnace and heated under vacuum to 1200°C for 1 hour. Following this, there were no signs of the sample reacting with the alumina, but it still appeared inhomogeneous.

From these tests, it is apparent that $ErIn_3$ can be melted in an alumina or tantalum crucible without reacting, but this simple melting does not seem to produce a homogeneous melt.

## *2.9 Conclusions*

Studying the properties of the $(Ho_xEr_{1-x})In_3$ samples is not a simple task because many different factors affect the properties. There is definite evidence that the low temperature heat capacity of $ErIn_3$ is dependent on the indium concentration. However, there appears to be no indium solubility in $HoIn_3$ as variations in indium do not affect the heat capacity. The indium concentration also has an influence on the $(Ho_xEr_{1-x})In_3$ samples, but seems to play a role only in the low holmium samples. The anomalous data within this series of materials do not appear to be the result of only indium, but could be the result of other impurities, or some other factor not yet identified.

Substituting other rare earth elements for erbium in $ErIn_3$ showed that a wider range of heat capacity peak temperatures might be possible. Low concentrations of yttrium appeared to have little to no effect on the heat capacity, while cerium and praseodymium lower the heat capacity peak but at a serious cost of magnitude. The $(Dy_xEr_{1-x})In_3$ system shows potential within the same temperature range as the $(Ho_xEr_{1-x})In_3$ system and might perhaps have a wider range of usefulness due to the higher Néel temperature of $DyIn_3$.

Deformation and stress also plays a big role in the properties of $ErIn_3$. Although the ductility is not high enough to be measured, the samples will deform under stress. This results in a

broadening in both the Bragg peaks and the heat capacity peaks. In order for $ErIn_3$ to be useful as a low temperature regenerator matrix material, it must be heat treated after forming.

$ErIn_3$ can be prepared within a tantalum or alumina crucible without reacting with the crucible, but further work needs to be done to ensure that a homogeneous mixture can be obtained.

# References

[1]. A. Iandelli, Atti accad. naz. Lincei, Rend. Classe sci. fis. mat. nat. 2 (1947) 327

[2]. R. Vogel and H. Klose, Z. Metallkd., 45 (1954) 633

[3]. A. Iandelli, Atti accad. naz. Lincei, Rend. Classe sci. fis. mat. nat. 29 (1947) 62

[4]. N. C. Baenziger and J. L. Moriarty, Jr., Acta Cryst., 14 (1961) 948

[5]. Yu. B. Kuz'ma and V. Ya. Markiv, Kristallografiya, 9 (1964) 279

[6]. J. L. Moriarty, R. O. Gordon, and J. E. Humphreys, Acta Cryst. 19 (1965) 285

[7]. I. R. Harris and G. V. Raynor, J. Less-Common Metals, 9 (1965) 7

[8]. J. L. Moriarty, J. E. Humphreys, R. O. Gordon, and N. C. Baenziger, Acta Cryst. 21 (1966) 840

[9]. K. H. J. Buschow, H. W. de Wijn, and A. M. van Diepen, J. Chem. Phys., 50 (1969) 137

[10]. G. Arnold and N. Nereson, J. Chem. Phys., 51 (1969) 1495

[11]. E. E. Havinga, H. Damsma, and M. H. van Maaren, J. Phys. Chem. Solids, 31 (1970) 2653

[12]. N. Nereson and G. Arnold, J. Chem. Phys., 53 (1970) 2818

[13]. S. Delfino, A. Saccone, and R. Ferro, J. Less-Common Metals, 65 (1979) 181

[14]. S. P. Yatsenko, A. A. Semyannikov, H. O. Shakarov, and E. G. Fedorova, J. Less-Common Metals, 90 (1983) 95

[15]. S. Delfino, A. Saccone, and R. Ferro, J. Less-Common Metals, 102 (1984) 289

[16]. A. Saccone, S. Delfino, and R. Ferro, CALPHAD, 14 (1990) 151

[17]. H. Okamoto, *Phase Diagrams of Indium Alloys and Their Engineering Applications*, C. E. T. White and H. Okamoto (eds.), Indium Corporation of America, Utica, N.Y., and Materials Information Soc., Materials Park, OH (1992)

[18]. R. Ackermann, *Cryogenic Regenerative Heat Exchangers*, Plenum Press, New York, NY (1997)

[19]. G. K. White and P. J. Meeson, *Experimental Techniques in Low-Temperature Physics*, Oxford University Press, NY 4th ed. (2002)

[20]. D. R. Gaskell, *Introduction to the Thermodynamics of Materials*, Taylor & Francis, Washington, DC, 3rd ed. (1995)

[21]. A. Daniels and F. K. du Pré, Triple-Expansion Sterling Cycle Refrigerator, Adv. in Cryogenic Engineering, 16, Plenum Press, New York (1971) 178

[22]. K. H. J. Bushcow, J. F. Olijhoek, and A. R. Miedema, Cryogenics, 15 (1975) 261

[23]. M. Sahashi, Y. Tokai, T. Kuriyama, H. Nakagome, R. Li, M. Ogawa and T Hashimoto, Adv. in Cryogenic Engineering, 35B, Plenum Press, New York (1990) 1175

[24]. T. Kuriyama, R. Hakamada, H, Nakagome, Y. Tokai, M. Sahashi, R. Li, O. Yoshida, K. Matsumoto, and T. Hashimoto, Adv. in Cryogenic Engineering, 35B, Plenum Publishing, New York, (1990) 1261

[25]. T. Biwa, W. Yagi and U. Mizutani, Jpn. J. Appl. Phys., 35 (1996) 2244

[26]. T. Satoh, A. Onishi, I. Umehara, Y. Adachi, K. Sato, and E. J. Minehara, "A Gifford-McMahon Cycle Cryocooler below 2K", Cryocoolers 11, Plenum Press, New York, NY (2001) 381

[27]. K. A. Gschneidner, Jr., A. O. Pecharsky, and V. K. Pecharsky, "Ductile, High Heat Capacity, Magnetic Regenerator Alloys for the 10 to 80 K Temperature Range", Cryocoolers 11, Plenum Press, New York, NY (2001) 433

[28]. A. Czopnik, H. Mädge and B. Staliński, phys. stat. sol. (a) 94 (1986) K13

[29]. K. A. Gschneidner, Jr., A. O. Tsokol, L. Hale, and V. K. Pecharsky, Advances in Cryogenic Engineering: Transactions of the International Cryogenic Materials Conference – ICMC, 52 (2006) 19

[30]. B. A. Hunter (1998) "Rietica – A visual Rietveld program", International Union of Crystallography Commission on Powder Diffraction Newsletter No. 20, (Summer) http://www.rietica.org

[31]. D. C. Jiles, *Introduction to Magnetism and Magnetic Materials*, Chapman and Hall, London and New York, NY 2nd ed. (1998)

[32]. V. K. Pecharsky, J. O. Moorman, and K. A. Gschneidner, Jr., Rev. Sci. Instrum. 68(11) (1997) 4196

[33]. B. Staliński, A. Czopnik, and N. Iliew, Journal de Physique. 40 (1979) C5-149

[34]. P. Lethuillier, and J. Chaussy, Journal de Physique. 37 (1976) 123

[35]. V. K. Pecharsky and P.Y. Zavalij, *Fundamentals of Powder Diffraction and Structural Characterization of Materials*, Kluwer Academic Publishers, New York, NY (2003)

[36]. C. Kittel, *Introduction to Solid State Physics*, John Wiley and Sons, Inc. Hoboken, NJ 8th ed. (2005)